Product Engineering for Man-Portable Power Generation Based on Fuel Cells

Alexander Mitsos, Michael M. Hencke, and Paul I. Barton
Dept. of Chemical Engineering, Massachusetts Institute of Technology, Cambridge, MA 02139

DOI 10.1002/aic.10456
Published online May 19, 2005 in Wiley InterScience (www.interscience.wiley.com).

Microfabricated fuel cell systems are a promising alternative to batteries for man-portable power generation. These devices are potential consumer products that constitute a more or less complex chemical process, and can therefore be considered chemical products. A great variety of potential devices are being considered in various research institutions and thus there is a need for a systematic product design methodology, including comparison of alternatives and examination of the influence of technological parameters. The design of these product/process hybrids is inherently different from macroscale process design because of the differing design specifications, objectives, and constraints, as well as the relative importance of the underlying physico-chemical phenomena. Heat losses substantially influence the process performance, so the processes are highly spatially integrated. Consequently, flowsheet design and layout need to be considered simultaneously. In this paper we present our methodology and perform a number of case studies, including studies of scaling of the processes and effects of layout options and relevant technological parameters. © 2005 American Institute of Chemical Engineers *AIChE J,* 51: 2199–2219, 2005

Keywords: man-portable power, micropower generation, product engineering, fuel cell system, SOFC, PEM, PCFC, DMFC, products that are processes, microfabricated fuel cell

Introduction

The ever-increasing use of portable electric and electronic devices increases the need for efficient autonomous man-portable power supplies.[1,2] Currently, batteries are the predominant technology in most applications. However, batteries have a substantial environmental impact, high cost, and relatively low gravimetric (Wh/kg) and volumetric (Wh/L) energy densities. State-of-the-art primary batteries reach up to 1300 Wh/L and 700 Wh/kg and rechargeable up to 400 Wh/L and 300 Wh/kg.[3,4] The upper limit on battery performance is now being reached as most of the materials that are practical for use as active materials in batteries have already been investigated and the list of unexplored materials is being depleted.[2,3]

Correspondence concerning this article should be addressed to P. I. Barton at pib@mit.edu.

© 2005 American Institute of Chemical Engineers

There is both military[5] and civilian interest in alternative power generation. Out of the many technologies that are theoretically possible, microfabricated fuel cell–based systems have attracted much interest in recent years because fuel cells have the capability of achieving high efficiency, have few or no moving parts, and run silently. Companies such as Motorola, Toshiba, Casio, NEC, and Sanyo have research projects with the aim of developing miniature fuel cells[6,7] and several multidisciplinary research projects exist at universities, such as MIT[8] and UIUC.[9]

There are two main approaches for fuel cell systems: (1) direct fuel cells running on stored hydrogen, methanol, formic acid, or medium-sized hydrocarbons; and (2) fuel processing for hydrogen or syngas generation and subsequent oxidation of these intermediates in a fuel cell. Micropower generation devices based on either approach are products that constitute a more or less complex chemical process. There is a plethora of possible processes and process combinations, as well as a wide

variety of applications and consumers, ranging from cellular phones and laptops for home use to the power needs of the dismounted soldier; thus it is plausible that the optimal device configuration will depend on the product specifications characterizing particular applications. This necessitates a flexible methodology for the comparison of different technology alternatives that can facilitate product engineering of these devices. Since our preliminary study,[10] various articles dealing with modeling aspects[11-13] have appeared, although their focus is on detailed modeling of specific device designs rather than a comprehensive investigation of the system-level issues.

In macroscale processes plant layout is typically addressed independently of, and subsequently to, the design of the flowsheet; the main considerations for the layout are flow-driving forces from one unit operation to another (which sometimes leads to unit operations positioned with a height difference) and sufficient spatial separation (for safety reasons). This decomposition strategy—which is possible because the unit operations are virtually independent from each other—relies on an effective means of transferring heat between units, a problem that is solved with the methodology of heat-exchanger network synthesis.[14] At the microscale, on the other hand, the process components are highly integrated and heat losses significantly influence the process performance[10] and possibly the optimal design, so that the problems of flowsheet design, physical layout, and integration of heat sinks and heat sources need to be addressed simultaneously. A very promising approach is to couple two or more unit operations thermally in a near-isothermal stack.[15]

The devices considered need to operate independently of external heat sources, despite, say, the use of endothermic fuel processing reactions or high operating temperatures that lead to high heat losses. The simplest approach to provide the necessary heat is to use part of the fuel in a combustion or catalytic oxidation reaction, although a more promising approach is to use a fuel combination. The motivation is that one fuel can be used for reforming (hydrogen production) and another for combustion/heat generation. Using multiple fuels is of particular interest in the case that a low energy-density fuel (such as ammonia or methanol) is used for hydrogen production, especially when an endothermic reaction is used (such as cracking).

The study reported here builds on the preliminary study,[10] considering a significantly increased set of possible processes; examples include more fuel options, allowing fuel combinations, more fuel cell types, and more recycling options. The models are more detailed while remaining general enough to be independent of the geometry and catalysts used; examples of increased detail are the calculation of system energy densities as opposed to fuel energy densities and considerations of water permeation. A completely new contribution is the introduction of idealized layout options, which allows for simultaneous flowsheet and layout design without specifying a detailed geometry; this is necessary because of the pronounced effect of heat losses at the microscale. The case studies clearly show that product specifications and advances in technology influence not only the process performance but also the optimal design.

Product Specifications

Micropower-generation devices can be considered chemical products because they affect chemical change.[16] Unlike traditional chemical products, their characteristics do not depend on the molecular structure or microstructure but rather on the performance of the underlying chemical and electrochemical unit operations. Most of the methodologies proposed for product design[16-19] include a step identifying the customer's needs before inventing and analyzing alternative products that can fulfill these needs. The final step in product design is to analyze the manufacturing alternatives to make this product, which, in the case of micropower-generation devices, calls on MEMS (micro-electro-mechanical systems) fabrication technology. Although this paper focuses on a methodology for comparison of fuel-cell–based device alternatives, in this section we briefly characterize the product specifications for different applications. Manufacturing of the devices is not the topic of this paper, but the alternatives considered are limited based on manufacturing considerations.

There are several metrics for the assessment of portable power-generation devices and, depending on the application, they can be formulated as design objectives or constraints. For most applications, design objectives include minimizing weight and/or volume of the power generation device plus fuel. An interesting differentiation is between rigid and flexible volumes: for certain applications a flexible shape is desirable; for other applications a collapsible fuel container could be useful, so that the volume is reduced with time. The lifetime (measured in hours) of operation before the device needs replacement, recharging, or refueling can be either a design objective or constraint. Economical and environmental costs are important criteria that are dominated by the materials used in devices and the fabrication and recycle/disposal of processes, rather than the fuel used, and therefore are not the topic of this paper. Design constraints include reliability, safety, and flexibility to ambient conditions. Reliability should in general be at least as high as that of the devices one wants to power. From a consumer's perspective, the power-generation device must have a relatively simple way of recharging, refueling, or replacing. Power generation is coupled with heat generation arising from irreversibilities; the heat generation increases as the overall system efficiency decreases.[20] For highly inefficient processes the heat generation can render the device uncomfortable or even unusable, such as a cellular phone getting hot or an undesired heat signature in the battle field. For rechargeable and refuelable devices an important metric is the maximal number of operating cycles, as well as the performance degradation with increasing number of cycles.

A substantial number of devices, with different characteristics, currently require man-portable power production. Cellular phones currently use Li-ion rechargeable batteries with a mass of about 100 g, a cost of around \$20, standby operation of many hours, and runtime of at most a few hours. Digital camcorders have a power demand of a few watts and typically use rechargeable batteries with a cost of \$20–50. Laptop computer batteries are rechargeable (typically Li-ion), have a mass of at most a few kilograms, and typically have a capacity of under 100 Wh/kg, resulting in a few hours of power supply at around 5–10 W; they cost around \$100–200 and have a lifetime of nearly 300 charge/discharge cycles. Flashlights and toys operate with different types of batteries, either rechargeable or primary, with a power supply of 1–10 W; the battery weight and operating time vary significantly with an operating cost on the order of \$5/h. On the limit of portability are

electrical vehicles for the elderly and handicapped, which typically use lead–acid rechargeable batteries with a mass of several kilograms and a mission duration of many hours. It is to be expected that in the near future new power-consuming devices, with possibly drastically different specifications on the power demand, will come to the market. An example is so-called exoskeletons (also dubbed power pants, power elbows, etc.): robotic suits with the promise of multiplying the force of soldiers or rescue workers or even allowing motion to disabled people.[21-23] These devices will probably be characterized by a very low power demand during stand-by operation, for monitoring purposes, and a spike in the power demand, reaching tens or hundreds of watts during the actual operation. Other power-consuming devices that are likely to become interesting applications for man-portable power generation include portable medical devices and robots.

Both the power-consuming device and the customer influence the specifications on the power-generation device and, because potential customers range from children to a dismounted soldier, there is a great variety of needs. Power-generation devices for children need to be inherently at least as safe as current batteries and nontoxic, even when operated in a manner different from that specified; the price is very important, whereas the performance and reliability are not crucial. Men and women in business, wanting to travel with their electronic devices, need power-generation devices that can be carried and operated on airplanes, and refueling in different countries must be possible; performance and reliability are more important than price for this potential customer. Mountaineers need power-generation devices that can operate under extreme conditions for long mission durations; reliability is extremely important and performance largely outweighs price considerations. The dismounted soldier can be trained for safety and is already exposed to dangerous materials, and therefore safety requirements are less important than those in civilian applications; performance and reliability are the main criteria and cost considerations are almost negligible. Design constraints for the dismounted soldier may include operation without noise generation or a thermal signature, whereas operation under extreme conditions is possible.

Methodology

Most power-consuming devices are not operated constantly and have rapidly changing power demands, and therefore the dynamics and operation of power generation devices are very important. Similar to the electric vehicle application,[24] a fast start-up procedure, at most on the order of minutes, is required. Assuming that the devices will be able to respond rapidly to power demands, the average performance will most likely be dominated by the steady-state behavior of the devices. The comparison of alternatives discussed herein is therefore performed considering steady-state processes; the calculation of system energy densities is described in the Appendix.

Steady-state design at the macroscale is usually performed in stages,[14,25] by first specifying the input–output structure of the process, then the recycle structure, then the separation system, and finally the heat-recovery network. The physical layout is performed in the very late stages of process design. This hierarchical decomposition is possible because different units can operate independently from each other, a fact that has led to the unit-operations paradigm. At the microscale a different design paradigm is necessary: that of closely interconnected components of an integrated process. It is therefore necessary to consider heat integration and layout in the early stages of the process design together with the input–output structure.

We consider hundreds of alternative processes, chosen with the constraint that the realization of the processes is either currently under investigation or foreseeable in the short-term future (coming years). To describe the alternatives, we use a conceptual flowsheet superstructure (Figure 1), with the symbols explained below in Figure A1 of the Appendix. We want to emphasize that the superstructure is only conceptual, and several of the "units" can actually be physically combined. Our models account for thermal integration of the processes, as described in detail in the layout section of this article. Although kinetic data exist for special catalysts[11,26] that allow for detailed modeling, our intention is to have a general methodology that can cover various geometries and reactor types (PFR, CSTR, packed bed, and so on) and be independent of the specific catalysts used. Our models are thus based on user-specified efficiency parameters in the various units such as conversion, electrochemical efficiency, and separation efficiency. Once these parameters and the operating conditions have been specified, the performance of the system is calculated. As a consequence of the generality of the models, some important aspects cannot be addressed in detail; an example is the exact influence of the operating temperature on heat losses: on one hand, an increase in operating temperature increases the heat losses per unit surface area but, on the other hand, it also greatly increases the reaction rates and therefore decreases the size of the device. The physical properties used are described in Mitsos et al.[10] The implementation and convergence scheme is described in the Appendix.

The basic requirements for fuels are discussed in Mitsos et al.[10] The set of model fuels that we consider consists of ammonia, methanol, and propane/butane mixtures and we have also included compressed hydrogen as well as a relatively broad class of hydrogen generators, described in detail in the Appendix. In terms of oxidizing agents we include atmospheric air, compressed oxygen, and compressed air as well as oxygen generators, which can offer a significant increase in volumetric energy density compared to that of compressed gases. The modeling of the oxygen generators is described in the Appendix.

The first design choice is to choose the fuel that will be used for power production and whether to perform fuel processing in a reactor or to directly feed the fuel to a fuel cell. Based on the process design heuristic for simplicity[27] the postulated superstructure contains only one reactor. The next design choice is whether this fuel or another fuel will be fed into a burner for heat generation. The heat produced from burners serves to compensate for stream preheating, heat losses, endothermic reactions, or even heating of the system at start-up.

Depending on the fuel-processing reaction a secondary feed of water or oxygen to the reactor is necessary. If desired, we can split part of the reactor products and burn it to supply heat, in which case a stream split is necessary. As described in Mitsos et al.,[10] simply recycling the reactor products does not seem a promising option and no recycling after separation is considered here.

Certain components, such as carbon monoxide, have delete-

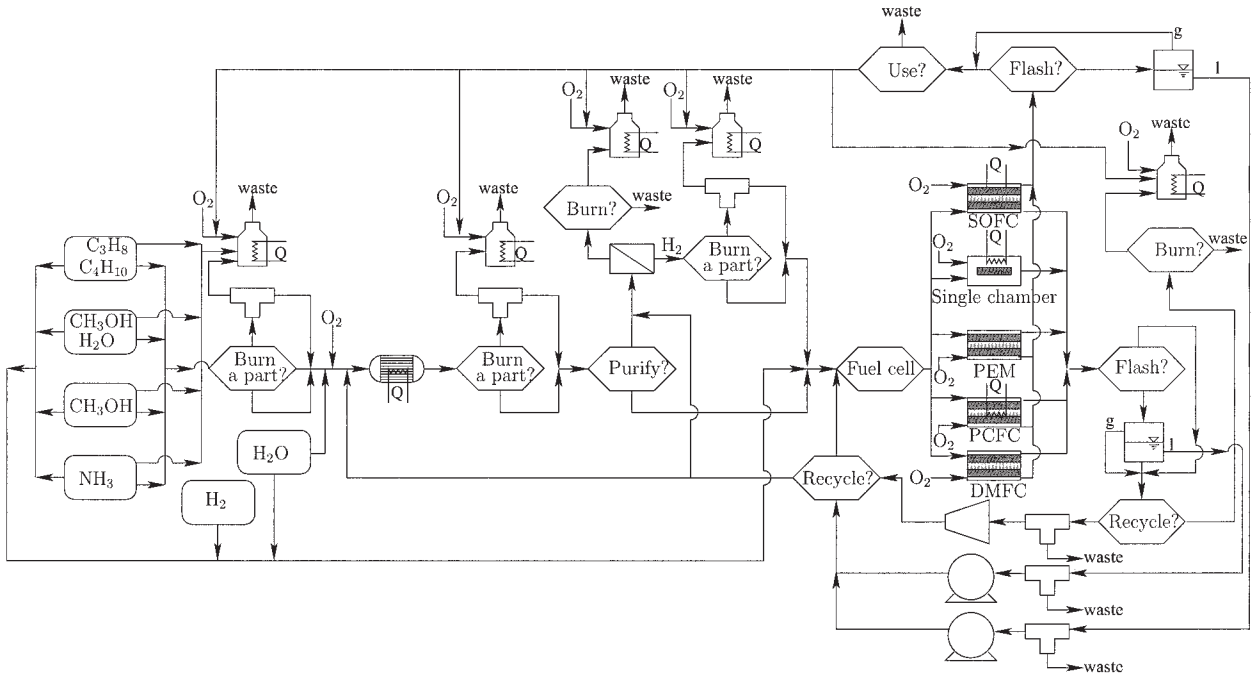

Figure 1. Conceptual process superstructure.

rious effects on some fuel cells [such as polymer electrolyte membrane (PEM)], and it may thus be necessary to perform a gas purification. We assume that the purification will lead to two streams, one of essentially pure hydrogen along with a waste stream. We consider a partial loss of the hydrogen in the waste stream, but we neglect any energetic penalty for the purification and the effect of a sweep stream, which may be necessary for the operation.[28] The purification could either be sequential to the reactor, or the reactor and the membrane could be combined into one unit, allowing for higher selectivity of the reactions toward hydrogen.[29,28] The separation waste can be either discarded or burned. If desired, the purification product (H_2) can be split, and a part can be fed into a burner.

We consider a variety of fuel cells: either a solid oxide fuel cell (SOFC) with the option of internal reforming; a proton ceramic fuel cell (PCFC); a hydrogen-operated PEM fuel cell; a single-chamber fuel cell operating with hydrogen and carbon monoxide; or finally a direct methanol fuel cell (DMFC). A SOFC has the benefit of fuel flexibility, although it is operated at a high temperature, which leads to substantial heat losses and problematic start-up. PEMs are run at low temperatures but cannot tolerate impurities, and water management is an issue. Single-chamber fuel cells are potentially easier to fabricate,[30] but have the drawback that they are operated with premixed gases that potentially can lead to explosions and require catalysts with high selectivity. A PCFC, which is a relatively new concept,[31] has the potential of fuel flexibility while operating at slightly lower temperatures than those of SOFCs. A DMFC is a PEM-based fuel cell in which a dilute methanol solution in water is reformed at a relatively low temperature, around 350 K; major technical challenges include methanol crossover and water management. The reader is referred to the literature for extensive discussions about the technology differences in the fuel cells.[32-34] Details concerning the fuel cell modeling used in this paper are found in the Appendix.

The conversion in the fuel cells (also denoted "fuel utilization") is not complete, and the unreacted part of the fuel can either be burned or recycled, and this basic recycling option was analyzed in Mitsos et al.[10] A more promising recycling option would be recycling after separation, such as separating the hydrogen of the fuel cell effluent and recycling it to the fuel cell, or separating the steam/water and using it for reforming reactions and to prevent coking. These options are very appealing from the perspective of minimizing the mass, but separation might be very difficult to implement in the general case. We allow for the option of separating the liquid and gaseous components of the anode and cathode effluents in a flash at a given temperature, most likely near-ambient, and recycling a fraction of the liquids (mainly water and methanol) to the reactor or the fuel cell anode. Depending on the implementation of the recycle stream, a pressure-increase mechanism may be necessary (such as a microfabricated pump), and we consider an energetic penalty in terms of a compression power. The remaining liquid components constitute a purge stream. The gaseous components can be recycled to the reactor, membrane, or fuel cell as in Mitsos et al.[10]

The cathode effluent stream of the fuel cell can be reused to provide oxygen for a burner because it is plausible that the fuel cells will be operated at a relatively large oxygen excess. Reusing excess oxygen is most advantageous in volume-critical applications where the oxygen cartridge may occupy a large fraction of the total system volume. In addition, the temperature of the cathode effluent stream is higher than the ambient, so this reduces the energetic requirement of preheating the oxygen feed to the burner. However, in circumstances where the fuel cell discard temperature is substantially lower than the operating temperature of the burner (that is, for a PEM or DMFC), preheating is still necessary. The cathode effluent also contains nitrogen, and in some cases (such as a PEM) steam, and heating of these components to the burner operating tem-

perature may outweigh the advantage of using preheated oxygen.

Integrated Layout and Thermal Management

The graphical representation of the superstructure (Figure 1) does not contain information about the physical layout. In Mitsos et al.[10] we demonstrated the pronounced effect of heat losses on process performance and the importance of thermal management for high-temperature micropower-generation devices. A very promising approach for thermal management is to thermally couple two or more units in a near-isothermal stack.[35] In this manner direct heat transfer between heat sinks and heat sources is possible, as well as heat recovery of the effluent streams; thermally coupling two units also reduces the surface area and, as a result, the heat losses. Combining units is thus a layout consideration that influences the process performance. As a consequence, the problems of flowsheet design, physical layout, and heat integration need to be solved simultaneously.

In the following description, we will refer to individual process components (that is, fuel cell, reactor, burner, and so on) as "units," although they are not independent in the sense of the unit-operations design paradigm. Specification of the process layout requires an indication of the relative location and connectivity of every unit present in the selected flowsheet of the superstructure, for example, is the fuel cell in thermal contact with the reactor? We propose an idealization of the layout considerations, allowing for only two extremes, implemented using logical decisions for the connectivity of each pair of units; this simplification is made for the same reasons that we used generic models for the reactor and the fuel cells. One extreme is that the units are thermally connected, so that they share the surface that results in heat losses, and one energy balance is sufficient. Within these "stacks," flow streams proceed directly between units, so that heat losses between units are neglected. Because of the small length scales associated with these microdevices, conduction is rapid in these stacks, thus necessitating that all units within a given stack operate with small temperature differences between them. Although our models allow for unit operating temperatures to be defined separately, this temperature constraint must be considered when deciding to combine two units. It is unlikely to find a way to use the heat excess of units operating at low temperatures, such as PEM or DMFC, and thus we do not allow the possibility of connecting these units with any other units. The combination of units may also be limited by fabrication possibilities that are not the subject of this study.

The other extreme that we consider is that the units are separated, so that each one has separate heat losses to the ambient and significant heat losses occur when mass or heat is transported between the units. In the case of a stream flowing from unit i to unit j, the temperature inlet to unit j is calculated as

$$T_j = T_i - \chi_{temp}(T_i - T_{amb})$$

where the energetic penalty ("temperature loss factor") $\chi_{temp} \in [0, 1]$ is a given parameter. In addition, heat exchange is inefficient, if not impossible, if the units are not integrated into stacks. We do allow for the option of heat exchange from burners that are not thermally coupled to the heat sink, but we impose an energetic penalty. The heat input to unit j is taken as a fraction of the heat output from unit i

$$Q_{j,in} = (1 - \chi_{heat})Q_{i,out}$$

and the difference between $Q_{i,out}$ and $Q_{j,in}$ is assumed to be lost to the ambient. We do not account for details of the heat exchange; possible realizations of heat exchange are radiation or conduction along a rod connecting the units, or preheating of inlet gases to one unit by the heat excess of the other. The parameters χ_{heat} and χ_{temp} are design dependent.

In Figure 2 the two extreme cases of layout are illustrated for a process in which butane is partially oxidized and the syngas produced is fed into a SOFC, whereas the cathode effluents are used to oxidize the unburned syngas from the anode for heat generation. In one extreme case the SOFC, reactor, and burner are assumed to be thermally coupled, whereas in the other extreme case, all three units are separate, with remote heat exchange between the burner and the SOFC. It should be noted that Figure 2 is conceptual and not an actual design.

Although layout options including many stacks are conceivable, we allow a maximum of two theoretical stacks, each of which can have up to five individual units. This restriction is motivated by the fact that the superstructure has up to two main units—the reactor and a fuel cell—and by this restriction an explosion in the number of logical choices is avoided. The five units potentially available for each stack are the fuel cell effluent burner, the membrane waste burner, the reactor, the fuel cell, and either a fuel burner (a reactor products burner) or a membrane products burner. We assume only one instance of the former four units and therefore they can be present in only one stack; we do allow for the possibility of splitting the fuel, reactor products, and membrane products streams, however, so that the latter units may be present in both stacks.

In the case that multiple burners are present in a stack, it is possible to combine them into a single unit, by mixing the inlet streams and producing a single waste stream. This may be easier from a fabrication perspective, or may result in a higher average conversion. According to the constraints on the number of units and stacks, there can be at most three burners in a single stack. In this case there are three possible ways to premix the burner streams: combine all three streams (one burner), combine two streams and leave the third stream separate (two burners), or leave all three streams separate (three burners). Our models allow for all three possibilities.

In our previous models,[10] we required that the system as a whole be autothermal (heat load negative or zero). We now impose the more detailed requirement that each stack be autothermal (heat load on each stack is negative or zero). Because we assume perfect heat exchange within the stack and heat exchange from noncoupled units subject to an energetic penalty, $\chi_{heat} \in [0, 1]$, the energy balance around a single stack with components i, inlet streams j, and outlet streams k is given by

$$\sum_i \sum_k N_{i,k}H_{i,k}(T_k) = \sum_i \sum_j N_{i,j}H_{i,j}(T_j) + Q_p - Q_{loss} + PW_{FC}$$

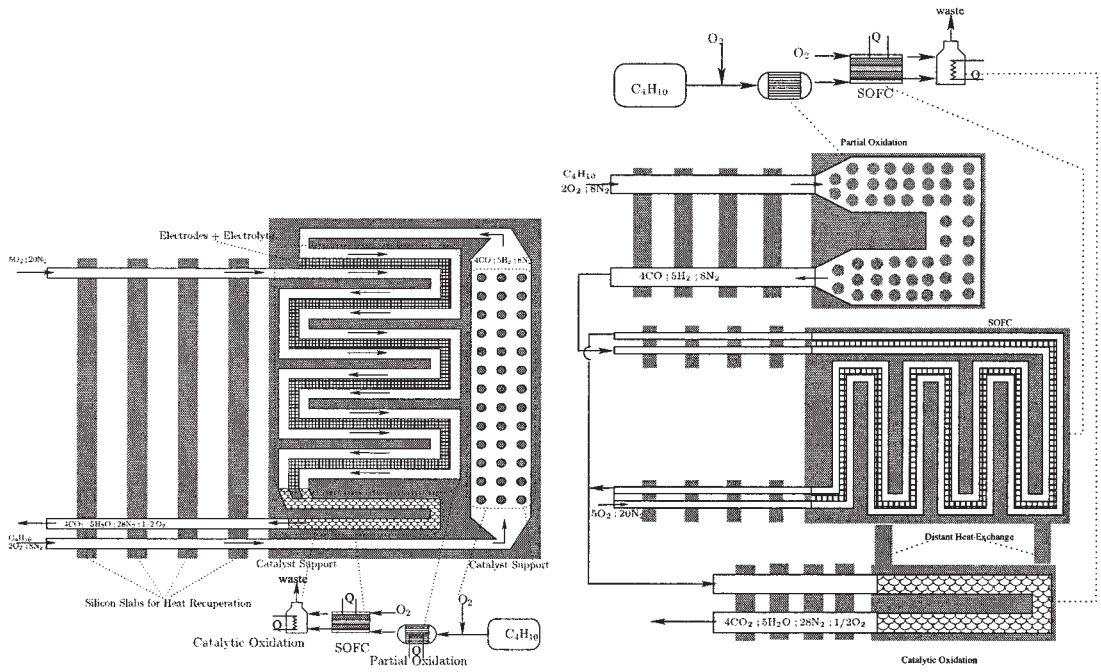

Figure 2. Conceptual difference between coupled (left) and noncoupled (right) process components.

We require that the sum of the heat duty Q_p of the stack and the effective heat exchange $(1 - \chi_{heat})Q_{remote}$ from remote units, is less than or equal to zero

$$Q_p + (1 - \chi_{heat})Q_{remote} \leq 0$$

In general heat removal can be problematic,[20,36] but we assume that for the processes considered it will be possible by reducing the insulation, introducing a heat sink element, or increasing the oxygen excess. We currently do not directly account for the (presumably small) decrease in the system performance by implementing these options.

In a similar vein to the combination of units, we also consider the option of combining fuel cartridges. This may be more difficult to fabricate, but has the advantage of minimizing the cartridge volume. We allow for the option of combining all fuel cartridges, combining the cartridges that go to burners, or keeping all the cartridges separate. In the case that compressed oxygen or an oxygen generator is used, we consider only the option of a single oxygen cartridge.

Case Studies

The number of processes considered is so large that an exhaustive comparison and study of the parameter dependency is not possible within the scope of this article. Instead, we choose to compare a small set of alternatives in terms of different metrics as well as to study the influence of key parameters (different for each alternative). These studies show the capabilities of the methodology developed and present insights into the product design of portable power-generation devices. It should be noted that the quantitative results depend on the values of the operating and modeling parameters used.

Influence of Product Specifications on Hydrides and Hydrocarbons

In Figure 3 we compare one SOFC-based and two PEM-based processes as a function of relevant technological parameters using two different metrics: volumetric and gravimetric energy density. For simplicity, we base the densities only on the amount of fuel needed, which dominates over the device size for long mission durations; these are referred to as gravimetric and volumetric *fuel* energy density, respectively. In the first process, denoted "Hydride," hydrogen is released by a hydride and fed directly into a PEM. For the gravimetric energy density we use a hydride density of 0.2 g H_2/cm^3 and vary the weight percentage of hydrogen, whereas for the volumetric energy density we use a value of 8 wt % and vary the hydride density. In the second process, denoted "POX-PEM," the propane/butane system is partially oxidized, and the hydrogen is separated with a varying recovery η_M and then fed into a PEM. Finally, in the SOFC-based process, denoted "POX-SOFC," the propane/butane system is partially oxidized and fed into a SOFC and the fuel cell effluents are used in a combustion chamber to provide sufficient heat for the high operating temperatures; the reactor, burner, and SOFC are assumed to be in thermal contact; carbon monoxide and hydrocarbons are assumed to be consumed in reforming reactions in the SOFC. For the PEM-based processes there is always heat excess and the decision of oxidizing the fuel-rich streams depends on the product requirements; they should be oxidized in an environment with strict requirements on toxic or dangerous emissions, and should not be oxidized when heat removal or heat signature are of concern.

Table 1 summarizes the parameters used. The main observation is that the optimal design depends on the relative importance of objectives, that is, maximal volumetric or gravi-

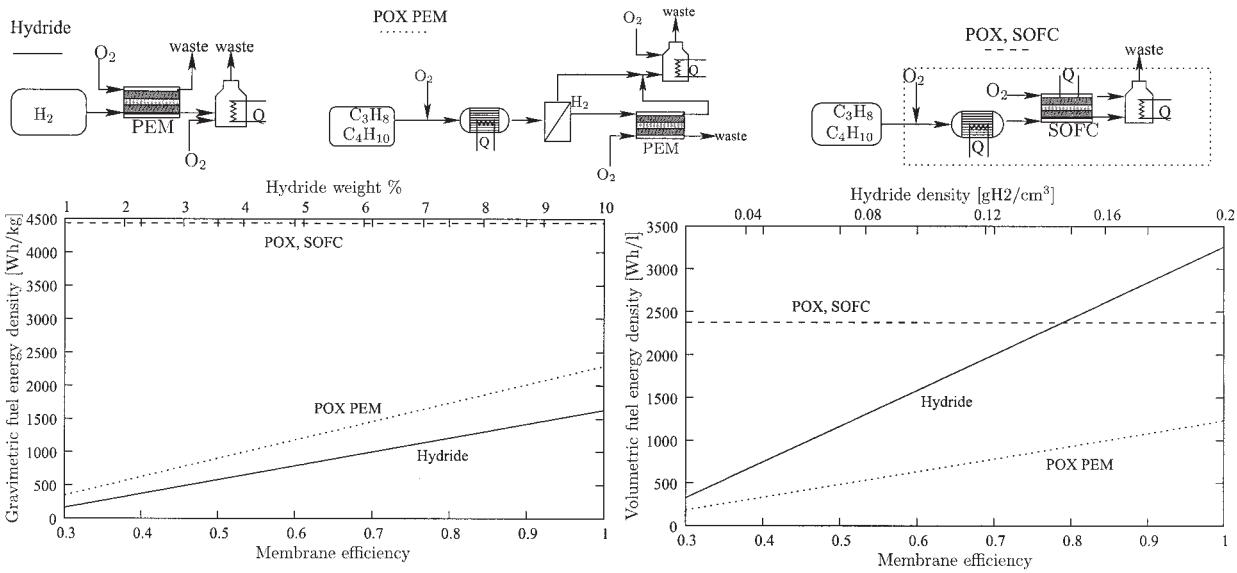

Figure 3. Comparison of hydride-based and hydrocarbon-based processes in terms of volumetric and gravimetric fuel energy density.

metric energy density, as well as advances in technology, that is, membrane efficiency and hydride density. It is therefore plausible that different applications will require a different power-generation device and that the optimal design can change with technological improvements. Regarding the actual comparison of hydrides and hydrocarbons, the qualitative behavior is that highly concentrated hydrides can compete with hydrocarbon-based processes in terms of volumetric energy density, whereas in terms of the gravimetric energy density they cannot. We reiterate that the exact numbers depend on the parameters used. Hydrogen recovery is very important but, even with complete recovery, the loss of the chemical potential of carbon monoxide makes PEM-based processes less attractive than those using a SOFC.

Although the exact device size depends on fabrication and packaging technologies, it is to be expected that the processes that use hydrocarbon processing will result in a larger device than hydride-based fuel cells because of the presence of a reactor. Therefore for small mission durations and/or power requirements the hydride-based processes might be the optimal choice. On the other hand, for longer mission durations and high power requirements, the fuel size dominates over the device size and one would expect that hydrocarbons will be the fuel of choice.

Effect of Oxygen Generators

In Mitsos et al.[10] we analyzed the effect of using compressed oxygen for cases where atmospheric air is not available (for underwater operations such as recreational diving). The volume of the compressed oxygen is very large and consequently the volumetric energy density is low. Here we compare the process of the previous design based on partial oxidation of propane/butane in combination with a SOFC for a mission duration $\tau_{mission} = 30$ h using either an oxygen generator or compressed oxygen as the source of oxygen. For the case of compressed oxygen we assume a plastic fuel storage material with a maximal allowable tensile stress of 100 MPa and a density of 1.5 kg/L and no minimum thickness requirement and we vary the storage pressure in the range 10–1000 bar. For the case of hydrogen peroxide we again use a cartridge density of 1.5 kg/L and vary the hydrogen peroxide weight fraction for two cartridge wall thicknesses, 1 and 10 mm. The properties for the storage materials were based on the range given in Perry

Table 1. Process Parameters for the Comparison in Figure 3

Ambient temperature	$T_{amb} = 298$ K	Power output	$PW = 1$ W
Reactor temperature	$T_{op} = 1000$ K	Reactor outlet temperature	$T_{out} = 500$ K
Conversion in reactor	$\zeta = 0.9$	SOFC temperature	$T_{op} = 1000$ K
Residence time in reactor	$\tau = 1$ ms	Discard temperature from SOFC	$T_{out} = 500$ K
Conversion in burners	$\zeta = 0.95$	PEM temperature	$T_{op} = 350$ K
Residence time in burners	$\tau = 1$ ms	Discard temperature from PEM	$T_{out} = 350$ K
Air excess in burners	$\Phi = 1.2$	Conversion in fuel cell	$\zeta = 0.8$
Overall heat loss coefficient	$U = 3$ W m^{-2} K^{-1}	Residence time in fuel cell	$\tau = 20$ ms
Emissivity (incl. view factor)	$\varepsilon = 0.2$	Efficiency of fuel cell	$\eta_{FC} = 0.7$
Air excess in fuel cell	$\Phi = 1.2$	Compression parameter for the air feed	$K_C = 10$ J mol^{-1} K^{-1}
Burner temperature	$T_{op} = 1000$ K	Discard temperature from burner	$T_{out} = 500$ K
Water factor in fuel cell	$\Psi = 1$	Propane molfraction in feed	0.5
No air excess in reactor	$\Phi = 1.0$		

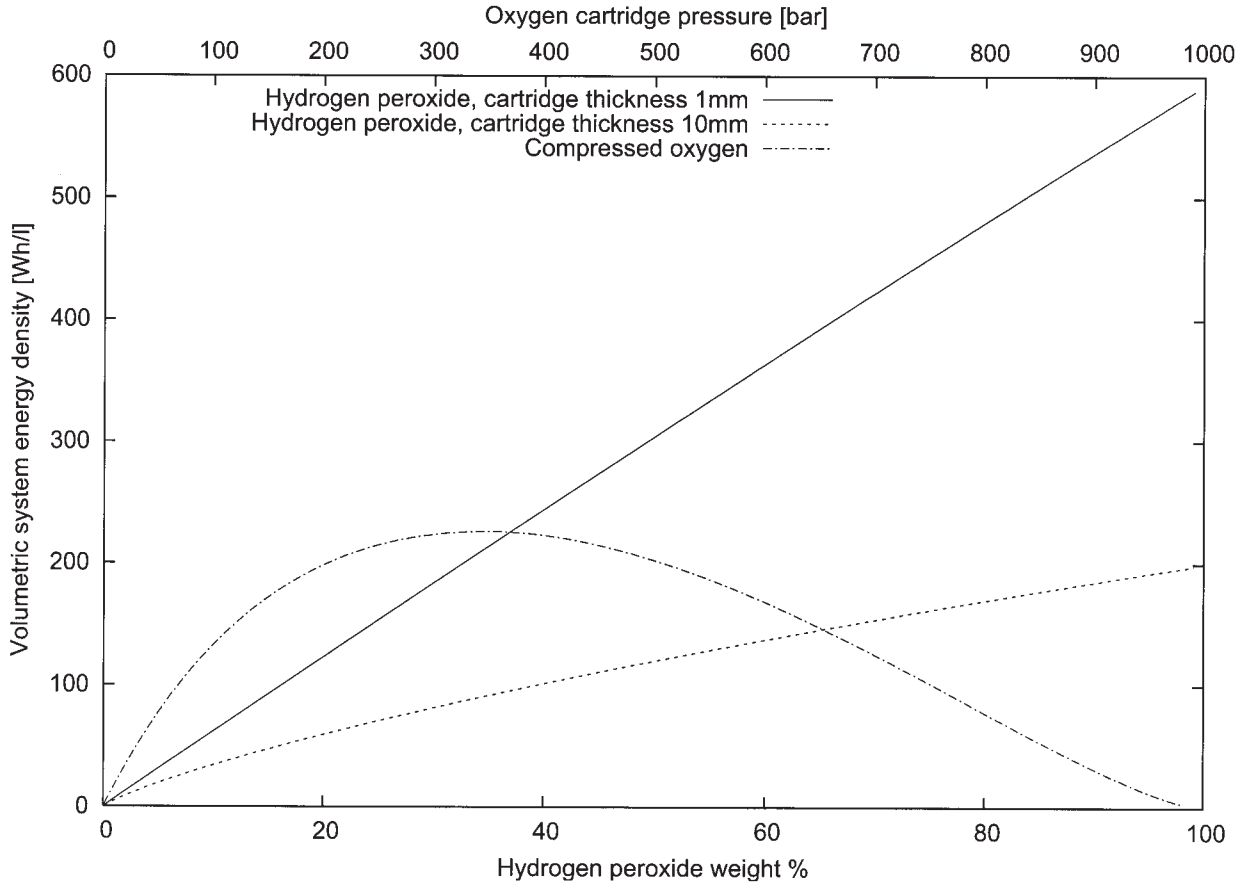

Figure 4. Comparison of hydrogen peroxide and compressed oxygen in terms of the volumetric system energy density.

and Green[37] for epoxic and polyesteric materials. As metrics for the comparison of the processes we use the volumetric and gravimetric *system* energy densities, where the system includes the power-generation device and the stored fuel, as described in the Appendix. Either metric can be more important depending on the application; for a mountaineer minimizing weight is more important than minimizing volume, whereas for a diver minimizing the mass is not as crucial because of buoyancy effects. The start-up time was assumed to be $\tau_{startup} = 60$ s with an auxiliary battery with a gravimetric energy density of 200 Wh/kg and a volumetric energy density of 200 Wh/L; the volume factor for the device is assumed to be 10 and the device density 1 kg/L. The influence of these parameters on the system volume and mass is insignificant, given that the volume and mass are dominated by the oxygen storage device.

In terms of the volumetric system energy density (Figure 4), relatively dilute oxygen generators can reach the performance of highly compressed oxygen. In terms of the gravimetric system energy density (Figure 5), only very concentrated hydrogen peroxide can outperform the compressed gas. The gravimetric system energy density in the case of compressed oxygen is decreasing with pressure because the required cartridge wall thickness increases superlinearly with the storage pressure, whereas the cartridge volume decreases linearly. The volumetric system energy density increases with storage pressure because of compression, but for greater pressure to allowable stress ratio the wall cartridge thickness increases so much that the cartridge volume becomes significant. In terms of the optimal product there is a trade-off between the safety requirement and the objective of minimizing weight and/or volume; safe operation requires thick cartridges and a dilute oxygen generator or moderate storage pressures, whereas energy density maximization requires a highly concentrated oxygen generator or high storage pressures using thin-walled cartridges. Depending on the relative importance of the objectives, either the oxygen generators or compressed oxygen may be the optimal choice. It can also be seen that the comparison with state-of-the-art batteries regarding the energy density is not very favorable and only highly efficient processes will be able to compete with batteries with respect to this metric.

Effect of Scale on Process Performance

The scalability of micropower-generation devices is particularly interesting because there are two major scales. One is the nominal power output, which is mainly associated with the device size, and the other is the time between refueling (mission duration), which is associated with the fuel cartridge size. In this case study we present the influence of these two scales on achievable system performance using the volumetric and gravimetric energy densities as metrics. We use the same parameters as in Table 1, a volume factor of 10, and a device

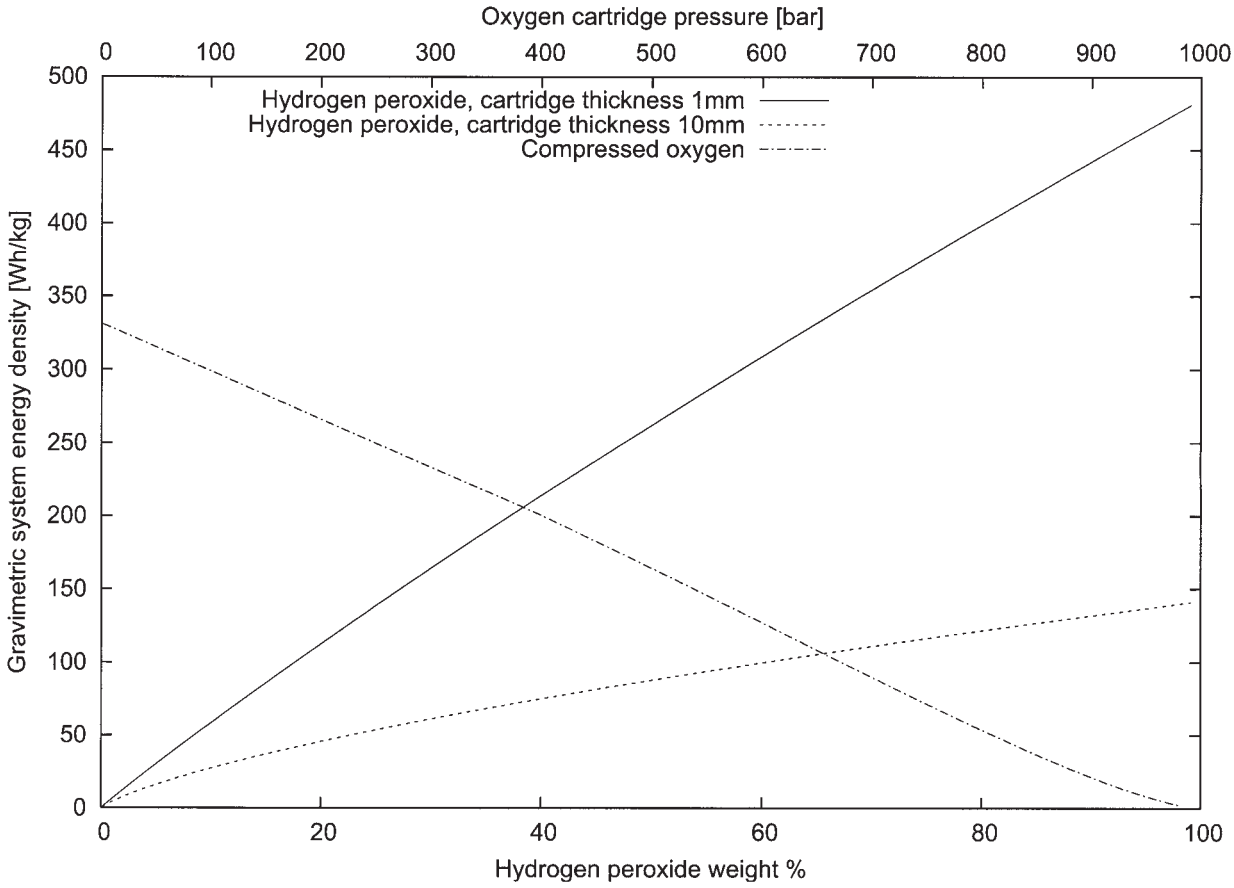

Figure 5. Comparison of hydrogen peroxide and compressed oxygen in terms of the gravimetric system energy density.

density of 1 kg/L. The fuel cartridge thickness was taken to be 1 mm and the density 1.5 kg/L. The start-up time was assumed to be $\tau_{startup} = 60$ s with an auxiliary battery with energy densities of 200 Wh/kg and 200 Wh/L. As metrics for the scalability we use the volumetric and gravimetric *system* energy densities, where the system includes the power-generation device and the stored fuel, as described in the Appendix. Figure 6 shows the achievable energy density in Wh/(L system) and Wh/(kg system) for the SOFC-based process.

For low power outputs the heat losses dominate over the

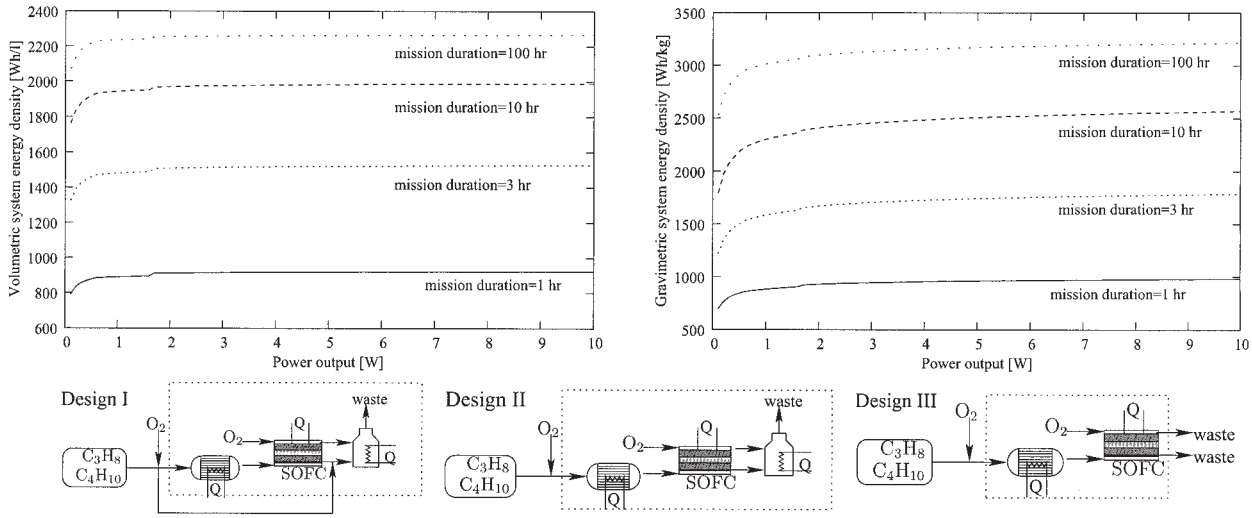

Figure 6. Volumetric and gravimetric system energy density of hydrocarbon partial oxidation in combination with a SOFC as a function of mission duration and power output.

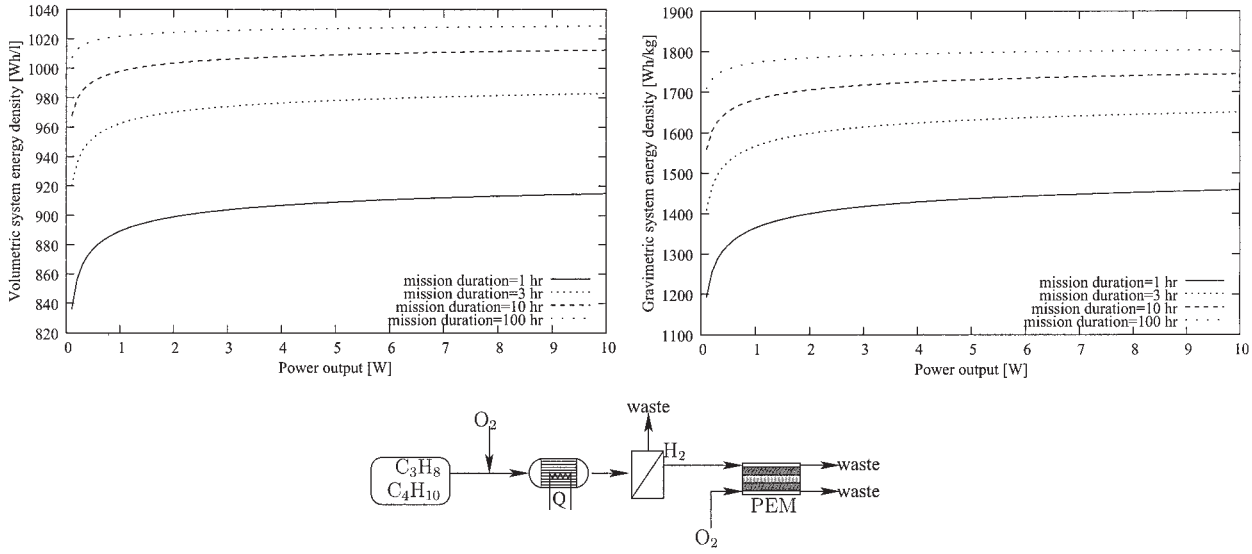

Figure 7. Volumetric and gravimetric system energy density of hydrocarbon partial oxidation in combination with a PEM as a function of mission duration and power output.

exothermicity of the fuel processing and burning of the fuel cell effluents as well as part of the fuel is needed (Design I). Because the heat generation scales linearly with power output, whereas heat losses scale sublinearly (with a power of 2/3), the achievable energy density increases significantly with the power output. At a power output of about 0.6 W a kink is observed because for higher power output the heat generation from burning the fuel cell effluents is sufficient (Design II). Above approximately 1.6 W the process is sufficiently exothermic, so that the fuel cell effluents need not be oxidized (Design III). It should be noted that these designs were obtained by comparing different designs through simulation rather than mathematical programming. The system energy density increases with mission duration and approaches the energy density with respect to the fuel volume/mass because the device size becomes negligible. This case study demonstrates that the influence of scale on process performance is significant; given that different processes generally scale differently, the optimal design is also likely to be influenced by the scale.

An interesting aspect regarding the performance of the individual "units" is their volumes, which determine the respective power density (W produced/volume). In this case study the fuel cell volume predominates over the volumes of the reactor and burner largely because of the residence times assumed. This volume ratio suggests that improvements in the fuel cell performance would have a much greater influence on device size than improving the reactor technology would. The power density for the SOFC is in the order of 700 W/L, whereas for the reactor approximately 15,000 W/L; it should be noted that these values are relative to the inner volume and do not include packaging of the devices.

The trend shown in Figure 6 is general and Figure 7 shows the scaling of the PEM-based process assuming a membrane efficiency of 0.8. The heat generated from the partial oxidation is sufficient to maintain the high operating temperature in the reactor and no oxidation of the membrane waste or fuel cell effluents is necessary from the perspective of heat balance; we here assume that emission of these gases is tolerated. The dependency on power output is mainly explained by the fact that small cartridges have relatively thicker walls than those of larger ones and is not as pronounced as in the SOFC case.

Effect of Fuel Combinations and Layout

In this case study we investigate the effect of using a second fuel for heat generation as well as how different layouts can yield significantly different system performances. A process that has been proposed[38] is ammonia decomposition to nitrogen and hydrogen and subsequent oxidation of the hydrogen in a PEM fuel cell. A major drawback of this process is that ammonia is corrosive and extremely toxic. From a technological perspective this process has the benefit that the ammonia does not contain carbon, and thus poisoning of the PEM can be avoided without the need for a separation after the fuel processing. However, the process has many drawbacks, including high operating temperatures for the fuel processing reactor and an endothermic fuel processing reaction, so that burning the fuel cell effluents may not provide sufficient heat.[10] Performance improvements can be achieved by the use of a second high energy fuel, such as hydrocarbons, for heat generation. We consider two extreme cases of layout: that either the two burners are separate and we have remote heat exchange or that the two streams to be burned are combined in a burner that is in thermal contact with the reactor. In Deschmukh et al.[11] it was demonstrated that conversion for the ammonia cracking reaction is essentially complete for residence times in the order of milliseconds and a fuel processing temperature of 650°C. Here we assume complete conversion of ammonia in the reactor and vary the residence time in the reactor in the range 0–100 ms. Table 2 summarizes the parameters used and Figure 8 shows the results in terms of the fuel energy density.

Even for low residence times combining units into a stack has a significant impact, and thermal integration seems necessary. This case study illustrates that flowsheet design and thermal management, including combination of heat sources and heat sinks, need to be considered simultaneously. The use

Table 2. Process Parameters for the Ammonia Cracking Case Study, Figure 8

Ambient temperature	$T_{amb} = 298$ K	Power output	$PW = 1$ W
Reactor temperature	$T_{op} = 923$ K	Discard temperature from reactor	$T_{out} = 623$ K
Conversion in burners	$\zeta = 0.95$	PEM temperature	$T_{op} = 350$ K
Residence time in burners	$\tau = 1$ ms	Discard temperature from PEM	$T_{out} = 350$ K
Air excess in burners	$\Phi = 1.2$	Conversion in fuel cell	$\zeta = 0.8$
Overall heat loss coefficient	$U = 3$ W m^{-2} K^{-1}	Residence time in fuel cell	$\tau = 20$ ms
Emissivity (incl. view factor)	$\varepsilon = 0.2$	Efficiency of fuel cell	$\eta_{FC} = 0.7$
Air excess in fuel cell	$\Phi = 1.2$	Compression parameter for the air feed	$K_C = 10$ J mol^{-1} K^{-1}
Burner temperature	$T_{op} = 1000$ K	Discard temperature from burner	$T_{out} = 500$ K
Temperature loss factor	$\chi_{temp} = 0.6$	Heat loss factor	$\chi_{heat} = 0.6$

of ammonia oxidation for heat generation in separate units becomes essentially impossible for long residence times because of the resulting increase in heat losses. The choice of a single fuel or a fuel combination is not obvious; from the perspective of maximizing the energy density the fuel combination is very advantageous, but it bears the logistic difficulties of carrying two fuels. This trade-off implies that for different applications a different design will be used.

Water Management in DMFC

It is well known that water management is a key consideration in direct methanol fuel cells.[34] Here we investigate the effect of internal (through diffusion from the cathode to the anode) and external (through flash separation of the fuel cell effluents) recycling of water. We use an operating temperature of $T = 350$ K, a conversion of methanol equal to $\zeta = 0.6$, a diffusion factor for hydrogen $k^{trns}_{H_2} = 1$, a methanol transport coefficient $k^{trns}_{CH_3OH}$, and a water factor $\Psi = 2$, as defined in the description of the DMFC model in the Appendix. The flash for the fuel cell effluents is assumed to operate at the ambient temperature $T_{amb} = 298$ K. As a figure of merit we use gravimetric *fuel* energy density, because we currently do not have accurate estimates for the sizing of mechanisms for external recycling, such as flash and pumps; in Figure 9 the

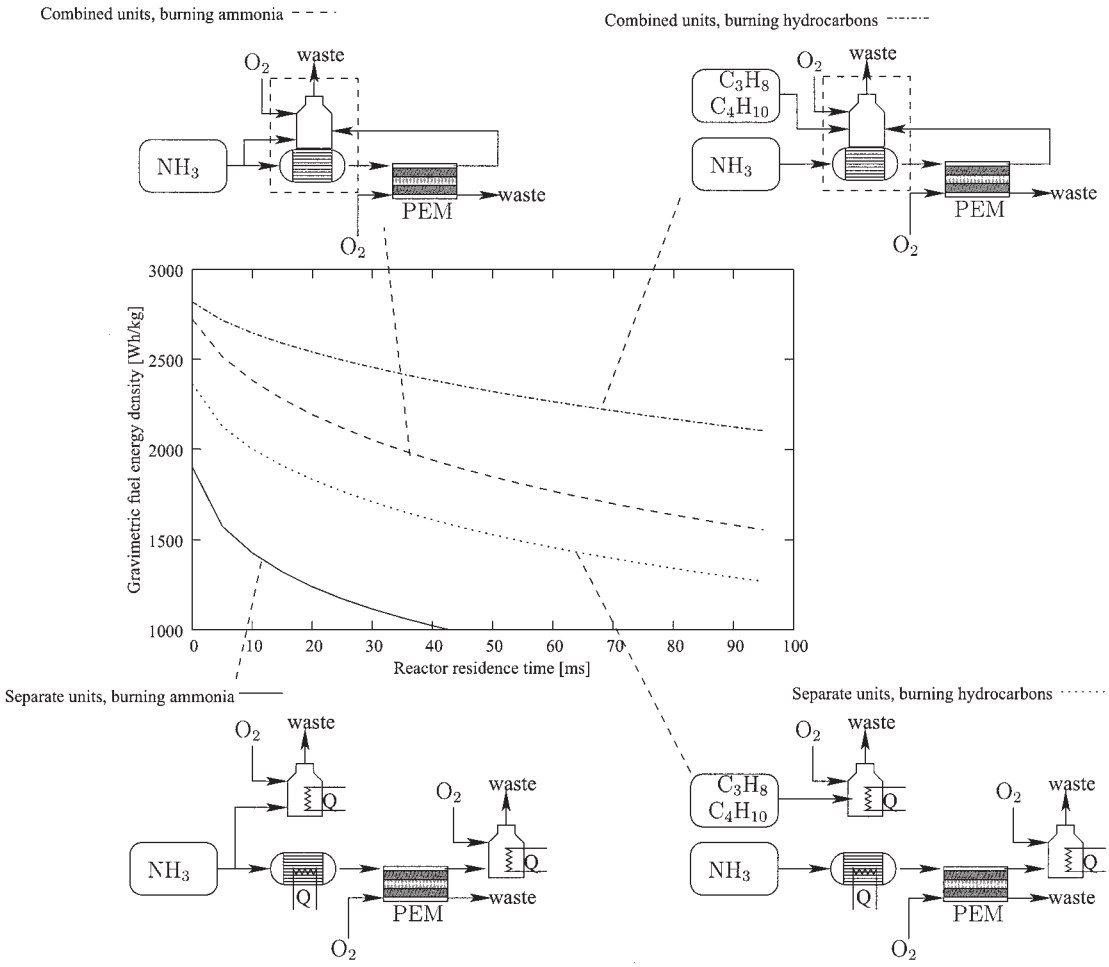

Figure 8. Effect of fuel combinations and layout options on gravimetric fuel energy density of an ammonia-cracking–based process.

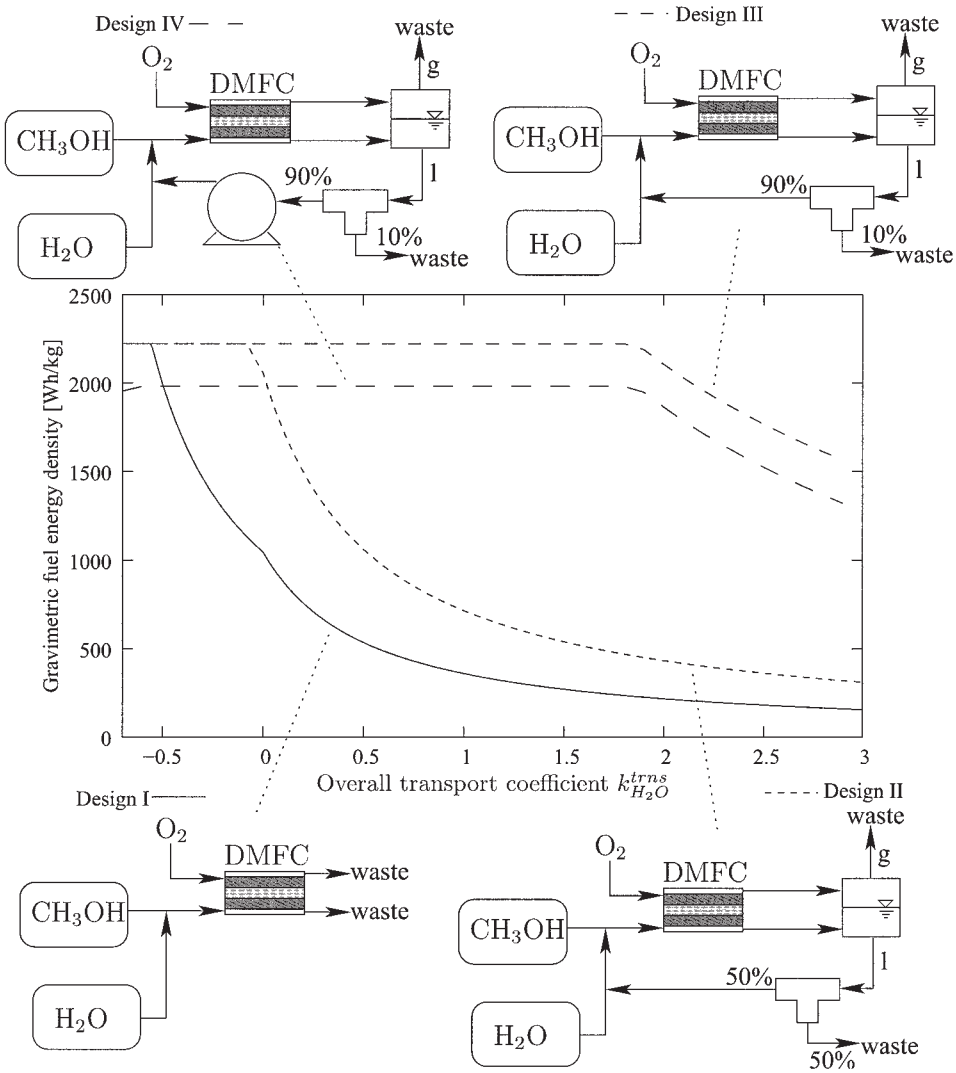

Figure 9. Effect of water recycling in a DMFC.

energy density is plotted as a function of the overall transport coefficient for water $k^{trns}_{H_2O} = -0.7$–3.

We consider four possible product designs. In the simplest case (Design I) no separation or recycling is performed, but rather the fuel cell effluents are directly wasted; in this case the energy density decreases substantially with increasing water transport coefficient, and the DMFC can operate efficiently only in the presence of internal recycling $k^{trns}_{H_2O} < 0$. Design II assumes that half of the liquid part of the fuel cell effluents can be recycled to the anode with a negligible energy penalty; again the energy density greatly depends on the water transport coefficient, but there is a wider range where the fuel cell can operate efficiently; for $k^{trns}_{H_2O} < 0$, the internal recycling provides sufficient water to the anode. Finally, for Designs III and IV we assume that effective external recycling can be achieved (90% of the liquid fuel cell effluents); in Design III without an energetic penalty and in Design IV with the extremely large energetic penalty of $K_P = 1 \times 10^5$ J/L; in both cases the fuel cell performance is efficient for a wide range of values for the water transport coefficient; the effect of the energetic penalty is relatively small because of the small volume of the liquid streams. For different values of the water excess factor Ψ, corresponding to a different composition of the fuel cell feed, the same qualitative behavior is observed with a shift in the achievable energy density and the range of values for the water transport coefficient. It should also be noted that although external recycling, if at all possible, can improve the process performance, there is a trade-off of increase in the device size and complexity. Whether recycling should be pursued depends on the product specifications and objectives, such as the power output and mission duration and the requirements on process performance, as well as on advances in the technology, such as the water transport coefficient.

Water Management in Water-Reforming Reactions

Steam reforming is widely used in stationary applications.[39] This is an interesting alternative because a water/steam system is relatively inexpensive, and in the case of fuel cells operating at high temperature the heat excess from the fuel cell can be used for the fuel processing reaction. In portable applications,

Table 3. Process Parameters for Water-Reforming Study in Figure 10

Ambient temperature	$T_{amb} = 298$ K	Power output	$PW = 1$ W
Reactor temperature	$T_{op} = 1000$ K	Reactor outlet temperature	$T_{out} = 1000$ K
Conversion in reactor	$\zeta = 0.9$	SOFC temperature	$T_{op} = 1000$ K
Residence time in reactor	$\tau = 10$ ms	Discard temperature from SOFC	$T_{out} = 500$ K
Conversion in burners	$\zeta = 0.95$	Residence time in burners	$\tau = 1$ ms
Air excess in burners	$\Phi = 1.2$	Conversion in fuel cell	$= 0.8$
Overall heat loss coefficient	$U = 3$ W m^{-2} K^{-1}	Residence time in fuel cell	$\tau = 20$ ms
Emissivity (incl. view factor)	$\varepsilon = 0.2$	Efficiency of fuel cell	$\eta_{FC} = 0.7$
Air excess in fuel cell	$\Phi = 1.2$	Compression parameter for air feed	$K_C = 10$ J mol^{-1} K^{-1}
Burner temperature	$T_{op} = 1000$ K	Discard temperature from burner	$T_{op} = 500$ K
Water factor in fuel cell	$\Psi = 1$	Pump parameter	$K_P = 100$ J/L
Propane molfraction in feed	0.5		

on the other hand, carrying the water significantly decreases the energy density, and therefore steam-reforming reactions are not necessarily the optimal fuel processing path. Water separation and recycling constitute a task that may be impossible to implement at the microscale, but it has the promise of significant improvements in performance because it can minimize the size of the water cartridge. On the other hand, reforming reactions are operated at relatively high temperatures, and therefore recycling of water is associated with a large energetic penalty for vaporization and heating; also recycling an excess of water dilutes the fuel and increases the required device volume, resulting in increased heat losses. The trade-off between these considerations leads to an optimum recycle ratio for a given requirement for water in the reactor feed.

Here we consider a process based on the combination of a hydrocarbon reforming reaction with a SOFC. The water re-

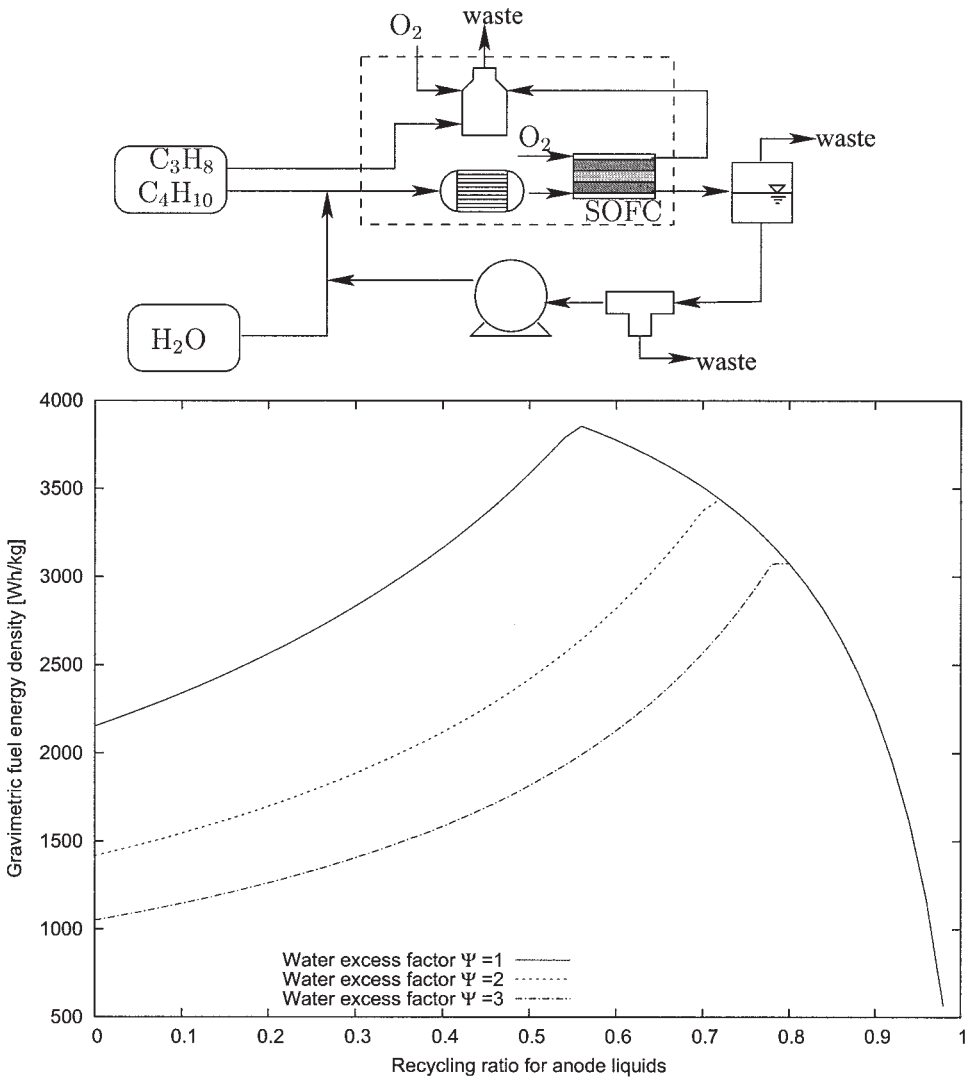

Figure 10. Effect of water recycling on the reforming reaction of hydrocarbons.

quirement in the reactor feed is specified according to an excess factor Ψ, relative to complete reforming reaction

$$N_{H_2O,in} \geq \Psi(3N_{C_3H_8,in} + 4N_{C_4H_{10},in})$$

The gaseous components after the flash separation are combusted, and the energy balance is closed by burning hydrocarbons. The reactor, fuel cell, and burner are assumed to be in thermal contact, and carbon monoxide and hydrocarbons are assumed to be consumed in reforming reactions in the SOFC. Table 3 summarizes the parameters used.

Figure 10 shows the effect of recycling for different stoichiometric compositions of the reactor inlet as a function of the recycle ratio. Because we consider a constant residence time, the reactor size increases for recycle ratios greater than the optimal one. Depending on value of the water factor Ψ, the optimum is observed at a recycle ratio of about 0.5–0.8. In a similar vein to the case of recycling in a DMFC there is a trade-off between an increase in the device size and complexity and the improvement of product performance.

Conclusions and Future Work

Micropower-generation devices based on fuel cells are products with the potential of outperforming batteries for man-portable power generation by an order of magnitude in terms of energy density. There is a plethora of conceivable applications and processes and this results in the need for product engineering. We have presented a methodology for the comparison of the alternatives and investigation of the influence of technological parameters. We have implemented the methodology as a tool available in the form of a web interface,[40] which allows for facile use by remote users who are unfamiliar with the modeling language and the details of the models. Upon request and subject to approval this web interface can be made available for academic purposes.

At the microscale, process components are highly integrated and the heat losses substantially influence the optimal design, so that the problems of flowsheet design, physical layout, and integration of heat sinks and sources need to be solved simultaneously. The optimal process design depends on product specifications and technological advances. The performance of water-consuming reactions depends strongly on the ability to separate and recycle the wastewater.

Under the assumption that rapid start-up is possible, the average performance mainly depends on the steady-state performance of the processes; nevertheless, the transient behavior is extremely important and needs to be addressed in the future. It is likely that certain processes exhibiting poor transient behavior must be excluded. It might also be necessary to oversize certain units relative to optimal steady-state design, or even add additional units with the sole purpose of start-up, such as a catalytic oxidation reactor to generate heat for start-up. These considerations lead to an interaction between the design and operation and we have started considering this.[41] The large number of flowsheet and layout options suggests that the application of mixed-integer (parametric) optimization techniques will lead to useful insights. Another important aspect is that of pressure considerations, including pressure drops and dependency of the process performance on the ambient pressure (such as that at high elevations). Currently, we have no good estimates for the size of peripheral devices, such as valves and pumps, but in contrast to the macroscale the energy consumption and influence of these components may be substantial and should be considered. Our modeling framework is flexible and we are considering the inclusion of more fuels, such as ethanol and formic acid,[42] or different fuel-processing mechanisms, such as autothermal reforming.[33]

Acknowledgments

This work was supported by the DoD Multidisciplinary University Research Initiative (MURI) program administered by the Army Research Office under Grant DAAD19-01-1-0566. We acknowledge Klavs F. Jensen and the other members of the MIT μChemPower team for fruitful discussions and their input in the formulation of the process alternatives.

Literature Cited

1. Jacobs R, Christopher H, Hamlen R, Rizzo R, Paur R, Gilman S. Portable power source needs of the future Army—Batteries and fuel cells. *IEEE AES Syst Mag*. 1996;11:19-25.
2. Dyer CK. Fuel cells for portable applications. *J Power Sources*. 2002;106:31-34.
3. Linden D. *Handbook of Batteries.* New York, NY: McGraw-Hill; 2001.
4. Brodd RJ. Recent developments in batteries for portable consumer applications. *Electrochem Soc Interface*. 1999;8:20-23.
5. Browning V. http://www.darpa.mil/dso/thrust/matdev/palmpower/index.html
6. http://www.space.com/businesstechnology/technology/ontheedge_0306.html
7. Mann C. Near-term nanotech. *Technol Rev*. 2004;22.
8. http://web.mit.edu/cheme/people/faculty/jensen.html
9. http://www.uiuc.edu/~r-masel/fuelcell/
10. Mitsos A, Palou-Rivera I, Barton PI. Alternatives for micropower generation processes. *Ind Eng Chem Res*. 2004;43:74-84.
11. Deschmukh SR, Mhadeschwar AB, Vlachos DG. Microreactor modeling for hydrogen production from ammonia decomposition on ruthenium. *Ind Eng Chem Res*. 2004;43:2986-2999.
12. Srikar VT, Turner KT, Ie T, Yung A, Spearing SM. Structural design considerations for micromachined solid-oxide fuel cells. *J Power Sources*. 2004;125:62-69.
13. Pattekar AV, Kothare MV. A microreactor for hydrogen production in micro fuel cell applications. *J Microelectromech Syst*. 2004;13:7-18.
14. Biegler LT, Grossmann IE, Westerberg AW. *Systematic Methods for Chemical Process Design.* Englewood Cliffs, NJ: Prentice Hall; 1997.
15. Arana LR, Schaevitz SB, Franz AJ, Schmidt MA, Jensen KF. A Microfabricated suspended-tube chemical reactor for thermally efficient fuel processing. *J Microelectromech Syst*. 2003;12:600-612.
16. Moggridge GD, Cussler EL. An introduction to chemical product design. *Chem Eng Res Des*. 2000;78:5-11.
17. Wibowo C, Ng KM. Product-centered processing: Manufacture of chemical-based consumer products. *AIChE J*. 2002;48:1212-1230.
18. Cussler EL, Wei J. Chemical product engineering. *AIChE J*. 2003;49:1072-1075.
19. Wei J. Molecular structure and property: Product engineering. *Ind Eng Chem Res*. 2002;41:1917-1919.
20. Meyers JP, Maynard HL. Design considerations for miniaturized PEM fuel cells. *J Power Sources*. 2002;109:76-88.
21. Huang GT. Wearable devices add strength. *Technol Rev*. 2004:26.
22. Huang GT. Wearable robots. *Technol Rev*. 2004:70-73.
23. Flowers W, McBean J, Narendran K. http://www.mit.edu/afs/athena/org/a/activejointbrace/index.shtml
24. Weber A, Ivers-Tiffée E. Materials and concepts for solid oxide fuel cells (SOFCs) in stationary and mobile applications. *J Power Sources*. 2004;127:273-283.
25. Douglas JM. *Conceptual Design of Chemical Processes.* New York, NY: McGraw-Hill; 1988.
26. Idem RO, Bakhshi NN. Kinetic modeling of the production of hydrogen from the methanol-steam reforming process over Mn-promoted coprecipitated Cu-Al catalyst. *Chem Eng Sci*. 1996;51:3697-3708.
27. Saha N, Rinard IH. Miniplant design methodology: A case study

manufacture of hydrogen cyanide. Proc of 4th Int Conf on Microreaction Technology (IMRET 4), Atlanta, GA, Mar. 5–9; 2000:327-333.
28. Franz AJ, Jensen KF, Schmidt MA. Palladium membrane microreactors. Proc of 3rd Int Conf on Microreaction Technology (IMRET 3), Frankfurt, Germany, Apr. 18–21; 1999:267-276.
29. Shu J, Grandjean BPA, Vanneste A, Kallaguine S. Catalytic palladium-based membrane reactors—A review. *Can J Chem Eng*. 1991;69: 1036-1060.
30. Dyer CK. A novel thin-film electrochemical device for energy conversion. *Nature*. 1990;343:547-548.
31. Coors WG. Protonic ceramic fuel cells for high-efficiency operation with methane. *J Power Sources*. 2003;118:150-156.
32. *Fuel Cells: A Handbook*. 5th Edition. San Diego, CA: EG&G Services, Parsons, Inc., Science Applications International Corporation; 2000.
33. Song C. Fuel processing for low temperatures and high temperature fuel cells. Challenges and opportunities for sustainable development in the 21st century. *Catal Today*. 2001;77:17-49.
34. Haile SM. Fuel cell materials and components. *Acta Mater*. 2003;51: 5981-6000.
35. Arana LR, Baertsch CD, Schmidt RC, Schmidt MA, Jensen KF. Combustion—Assisted hydrogen production in a high-temperature chemical reactor/heat exchanger for portable fuel cell applications. Proc of 12th Int Conf on Solid-State Sensors, Actuators, and Microsystems (Transducers 03), Boston, MA; 2003.
36. Maynard HL, Meyers JP. Miniature fuel cells for portable power: Design considerations and challenges. *J Vac Sci Technol*. 2002;20: 1287-1297.
37. Perry RH, Green DW. *Perry's Chemical Engineering Handbook.* http://www.knovel.com; 2002.
38. Metkemeijer R, Achard P. Ammonia as a feedstock for a hydrogen fuel cell; reformer and fuel cell behaviour. *J Power Sources*. 1994;49:271-282.
39. Farooque M, Maru HC. Fuel cells—The clean and efficient power generators. *Proc IEEE*. 2001;89:1819-1829.
40. Mitsos A, Hencke MM., Barton PI. http://yoric.mit.edu/micropower.html
41. Chachuat B, Mitsos A, Barton PI. Optimal operation and design of micro power generation processes. Proc of AIChE Annual Meeting, Austin, TX, Nov. 7–12; 2004.
42. Rice C, Ha S, Masel RI, Wieckowski A. Catalysts for direct formic acid fuel cells. *J Power Sources*. 2003;115:229-235.
43. Peters MS, Timmerhaus KD, West RE. *Plant Design and Economics for Chemical Engineers.* 5th Edition. New York, NY: McGraw Hill; 2003.
44. MSDS Hydrogen Peroxide. http://www.bu.edu/es/labsafety/ESMSDSs/MSHydPeroxide.html
45. LCSS Hydrogen Peroxide. http://www.hhmi.org/research/labsafe/lcss/
46. Goor G, Glenneberg J. Hydrogen peroxide. *Ullmann's Encyclopedia of Industrial Chemistry*. New York, NY: Wiley; 2000.
47. Easton MF, Mitchell AG, Wynne-Jones WFK. The behaviour of mixtures of hydrogen peroxide and water. *Trans Faraday Soc*. 1952; 48:796-801.
48. Züttel A, Wenger P, Sudan P, Mauron P, Orimo S. Hydrogen density in nanostructured carbon, metals and complex materials. *Mater Sci Eng*. 2004;B108:9-18.
49. Züttel A, Rentsch S, Fischer P, Mitsos A, Hencke MM, Barton PI. Hydrogen storage properties of $LiBH_4$. *J Alloys Compd*. 2003;356/357:515-520.
50. Slattery DK, Hampton MD. Complex hydrides for hydrogen storage. Proceedings of the 2002 U.S. DOE, Hydrogen Program Review http://www.eere.energy.gov/hydrogenandfuelcells/pdfs/32405b34.pdf
51. Heung LK. Using metal hydride to store hydrogen. Technical Report, Savannah River Technology Center. http://sti.srs.gov/fulltext/ms2003172/ms2003172.pdf; 2003.
52. Ren X-M, Springer TE, Zawodzinski TA, Gottesfeld S. Methanol transport through Nafion membranes. *J Electrochem Soc*. 2000;147:466-474.
53. Guo H, Ma C-F. 2D Analytical model of a direct methanol fuel cell. *Electrochem Commun*. 2004;6:306-312.
54. Lu GQ, Wang CY, Yen TJ, Zhang X. Development and characterization of a silicon-based micro direct methanol fuel cell. *Electrochem Acta*. 2004;49:821-828.
55. Reid RC, Prasunitz JM, Poling BE. *The Properties of Gases and Liquids.* New York, NY: McGraw Hill; 1987.
56. Tolsma JE, Clabaugh JA, Barton PI. Symbolic incorporation of external procedures into process modeling environments. *Ind Eng Chem Res*. 2002;41:3867-3876.
57. Tolsma JE, Clabaugh J, Barton PI. http://yoric.mit.edu/abacuss2/abacuss2.html
58. Tolsma J, Barton PI. DAEPACK. An open modeling environment for legacy models. *Ind Eng Chem Res*. 2000;39:1826-1839.
59. Tolsma JE, Barton PI. http://yoric.mit.edu/daepack/daepack.html

Appendix

Calculation of energy densities

When comparing the devices, with respect to batteries in terms of energy densities, it is necessary to consider the whole system, that is, the device including the process units, the packaging, the fuel, and the fuel cartridge. In our previous publication[10] we considered only the fuel and defined the energy density as the power output over the gravimetric or volumetric flow rate, as $PW/\Sigma_{i,j} MW_i N_{i,feedj}$. This metric has the advantage that it is independent of the mission duration, but is a valid approximation to the system energy density for only long mission durations when the fuel size dominates over the device size.

To calculate the system size (mass and volume) the mission duration $\tau_{mission}$, that is, the time period between refueling, needs to be specified. The required fuel volume/mass is the product of the mission duration and the volumetric/gravimetric flow rate. For supercritical components (N_2, O_2, H_2) the molar volume is calculated assuming ideal gas at a given storage pressure, whereas for subcritical components the liquid molar volume is used. For the supercritical components the storage pressure is a specified parameter, whereas for subcritical components it is calculated as a function of the ambient temperature. A cylindrical cartridge of a given aspect ratio is assumed. For liquids and solids a constant wall thickness is assumed, whereas for gases and subcritical components the wall thickness t is calculated according to the ASME Boiler and Pressure Vessel Code[43]

$$t = \frac{P/\sigma_A}{1 - 0.6P/\sigma_A}\frac{d}{2} + t_{\min} \qquad P/\sigma_A \le 0.385$$

$$t = \left(\sqrt{\frac{1 + P/\sigma_A}{1 - P/\sigma_A}} - 1\right)\frac{d}{2} + t_{\min} \qquad P/\sigma_A > 0.385$$

where d is the inner diameter of the cartridge and σ_A is the maximal allowable tensile stress, an input parameter. For the special cases of hydrogen and oxygen generators a different

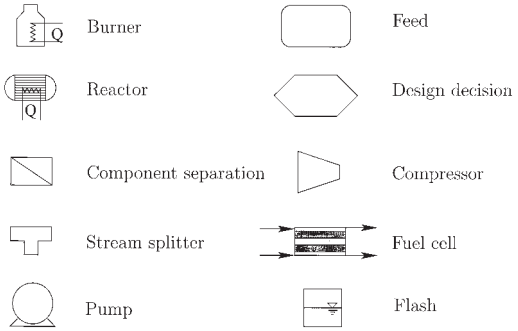

Figure A1. Explanation of the symbols used.

Table A1. Nomenclature

Abbreviation	Property	Unit
A	Surface	m^2
d	Cartridge inner diameter	m
e_{grav}^{bat}	Gravimetric energy density of auxiliary battery	Wh/kg
e_{vol}^{bat}	Volumetric energy density of auxiliary battery	Wh/L
$H_{i,j}$	Molar enthalpy of component i in stream j	J/mol
G_i°	Molar Gibbs free energy of pure component i at reference pressure	J/mol
$\Delta_r G$	Gibbs free energy of reaction r at system pressure	J/mol
k_i^{trns}	Transport coefficient for component i	(mol/s)/(mol/s)
K_C	Compressor parameter	J mol^{-1} K^{-1}
K_P	Pump parameter	J/L
M	Mass	kg
MW_i	Molar weight of component i	kg/mol
m_i	Mass of component i	kg
n_i	Mol number of component i	mol
n_{i0}	Initial mol number of component i	mol
$N_{i,j}$	Molar flow of component i of stream j	mol/s
$N_{i,diff}$	Diffusion rate of component i	mol/s
P	Pressure	bar
P_{ref}	Reference pressure	bar
PW	Power	W
Q_{loss}	Heat losses	W
Q_p	Heat load of unit p	W
$Q_{i,in}$	Heat exchange into unit i	W
$Q_{i,out}$	Heat exchange out of unit i	W
Q_{remote}	Heat exchange from remote units	W
R	Gas constant	J mol^{-1} K^{-1}
t	Cartridge wall thickness	M
T	Temperature	K
T_{amb}	Ambient temperature	K
U_{loss}	Overall heat loss coefficient	W m^{-2} K^{-1}
V	Volume	m^3
w_i	Weight fraction of component i	kg/kg
α	Split ratio	(mol/s)/(mol/s)
ε	Product of emissivity and view factor	$(W/m^2)/(W/m^2)$
η_{diff}	Diffusion efficiency	(mol/s)/(mol/s)
η_{ads}	Adsorption efficiency	(mol/s)/(mol/s)
η_M	Membrane efficiency	(mol/s)/(mol/s)
η_{FC}	Fuel cell efficiency	W/W
ζ_r	Conversion of reaction r	mol/mol
$\nu_{i,j}$	Stoichiometric coefficient of component i in reaction j	
ξ_r	Extent of reaction r	mol/s
ρ_i	Density of component i	kg/m^3
σ_A	Maximal allowable tensile stress	Pa
τ	Residence time	s
$\tau_{mission}$	Mission duration (time between refueling)	s
$\tau_{startup}$	Process startup time	s
Φ	Air ratio	(mol/s)/(mol/s)
χ_{temp}	Temperature loss factor	K/K
χ_{heat}	Heat exchange loss factor	W/W
Ψ	Water excess coefficient	(mol/s)/(mol/s)

calculation is undertaken, described in the respective subsections.

During the mission duration the mass of the fuel is constantly decreasing, whereas typical batteries have a constant mass, and the mass of zinc–air batteries increases with time as the metal is oxidized. We calculate both the initial and the average (1/2 the initial) fuel mass. We assume a rigid fuel cartridge and therefore the whole cartridge volume is considered. The device volume is estimated by calculating the necessary volume for the units and multiplying with a factor, order of magnitude 2–10, accounting for the volume necessary for the packaging of the devices. The device mass is then calculated with a given density.

It is most likely that the devices will be coupled with a relatively small, most likely rechargeable battery, for start-up and shutdown operations; the function of the battery will be to provide the required power and possibly to heat the fuel cell and reactor stack. We calculate the battery size based on a given start-up time period $\tau_{startup}$ and energy densities

$$M^{bat} = PW(\tau_{startup}/e_{grav}^{bat})$$

$$V^{bat} = PW(\tau_{startup}/e_{vol}^{bat})$$

Oxygen generators

In volume-critical applications where atmospheric oxygen is not available, chemical oxygen generators can offer a significant increase in volumetric energy density compared to compressed air or compressed oxygen. This increase in volumetric energy density, however, is coupled to a decrease in gravimetric energy density as a result of the added mass of the generator. We consider hydrogen peroxide as an example of such an oxygen generator. Because of its extensive current use, many of the safety concerns and transportation issues are already well understood.[44,45] No special regulations apply to the transport of dilute solutions ($\leq$8 wt %) of hydrogen peroxide, whereas concentrated solutions ($\geq$40 wt %) are not admitted for air transport.[46] Hydrogen peroxide decomposes when heated, releasing oxygen according to

$$H_2O_2^l \rightarrow H_2O^l + 0.5O_2^g$$

We consider a single cartridge that feeds all the units. For a given mission duration $\tau_{mission}$, the total moles and mass of hydrogen peroxide needed are given by

$$n_{H_2O_2} = 2\tau_{mission}N_{O_2,total}$$

$$m_{H_2O_2} = n_{H_2O_2}MW_{H_2O_2}$$

where $N_{O_2,total}$ is the molar flow of oxygen necessary for all units and the factor 2 comes from stoichiometry. For a given weight fraction of hydrogen peroxide ($w_{H_2O_2}$) in solution with water, the mass of solvent water is calculated as

$$m_{H_2O,solvent} = \frac{m_{H_2O_2}(1 - w_{H_2O_2})}{w_{H_2O_2}}$$

The total volume of solution is calculated as

$$V_{solution} = \frac{m_{H_2O_2}}{w_{H_2O_2}\rho_{solution}}$$

where the solution density $\rho_{solution}$ is assumed to depend linearly on the peroxide weight fraction[47]

$$\rho_{solution} = \rho_{H_2O} + w_{H_2O_2}(\rho_{H_2O_2} - \rho_{H_2O})$$

We do not account for the kinetics of hydrogen peroxide decomposition by assuming that they are sufficiently fast, nor do we account for the energy requirements by assuming that any required heat can be provided by ambient heat or by sweep gases from the fuel cell or reactor effluent streams.

Hydrogen generators

Using hydrogen as a primary fuel is an appealing alternative because of its high gravimetric energy density and the efficient operation of fuel cells with H_2. However, given that hydrogen is supercritical at ambient temperature, it cannot be liquefied and gaseous hydrogen storage requires a large volume, resulting in a low volumetric energy density. These limitations, along with difficulty in storage and safety issues of pure hydrogen, have led to the consideration of safer, low-volume and low-pressure methods of hydrogen storage. As with oxygen generators, these hydrogen generators offer significant increases in volumetric energy densities but impose a penalty in terms of gravimetric energy densities. We consider the option of generic hydrogen storage in a single model, approximating many technological alternatives based on either physisorption, such as metal hydrides or carbon nanotubes,[48] or even chemical hydrides that do not require the addition of water for decomposition.[49,50] As parameters we use the hydrogen density $\rho_{H_2} = g\text{H}/\text{cm}^3$ *storage* and hydrogen weight fraction w_{H_2}. The range for these parameters is known for common metal hydrides[48,51]

$$\rho_{H_2} \approx 0.02 - 0.2 \text{ g/cm}^3$$

$$w_{H_2} \approx 0.01 - 0.08$$

The mass of hydrogen m_{H_2} required over the mission duration is calculated as

$$m_{H_2} = \tau_{mission} N_{H_2} MW_{H_2}$$

where N_{H_2} is the flow rate of hydrogen required for the given power output. The mass of void hydrogen generator (that is, the residual hydrogen storage material) needed for the mission duration is determined by the hydrogen weight percentage

$$m_{H_2gen} = \frac{m_{H_2}(1 - w_{H_2})}{w_{H_2}}$$

This mass is constant and must be carried for the entire mission duration. The mass of stored hydrogen will decrease from m_{H_2} to zero as hydrogen is released over the course of the mission. The volume required to store the hydrogen generator depends on the density of hydrogen ρ_{H_2} and initial stored mass of hydrogen:

$$V_{H_2gen} = \frac{m_{H_2}}{\rho_{H_2}}$$

Similarly to the oxygen generators we do not account for kinetics or energy requirements.

Unit models

In this section we describe all the unit models that have been added or modified since the publication of the report by Mitsos et al.[10] (For the models of the reactor, burners, and membrane the reader is referred to Mitsos et al.[10]) For all fuel cells we assume that the produced fuel cell power (PW) is proportional to the Gibbs free energy of reaction for the electrochemical reactions

$$PW = \eta_{FC} \sum_r \xi_r \Delta_r G$$

where the Gibbs free energy of reaction is given by

$$\Delta_r G = \sum_i \nu_{i,r} \left[G_i^\circ(T) + RT \ln\left(\frac{P}{P_{ref}}\right) \right]$$

We neglect the mixing term because this would require knowledge of the composition along the fuel cell, which depends on the geometry. With the exception of the SOFC, only the final hydrogen reaction is considered to contribute to the produced power, by using the notion of equivalent hydrogen.[32] A heat balance over the fuel cell yields

$$\sum_i N_{i,outc} H_{i,outc}(T_{outc}) + \sum_i N_{i,outa} H_{i,outa}(T_{outa}) = \sum_i N_{i,inc} H_{i,inc}(T_{inc}) + \sum_i N_{i,ina} H_{i,ina}(T_{ina}) + Q_p - Q_{loss} + PW$$

where Q_{loss} is calculated as described in Mitsos et al.[10] In all fuel cells we allow for specification of a minimum water feed to the anode; this is calculated on the basis of the water required for complete reforming reactions and water permeation, multiplied by the water factor Ψ, a given excess parameter; this factor is defined for each fuel cell in the following subsections.

Proton Ceramic Fuel Cell (PCFC). In this type of fuel cell, oxygen vacancies in a ceramic membrane allow for protonic conduction from the anode to the cathode and water conductivity[31] allows for water management by diffusion from the cathode to the anode. We assume that the mechanism described for methane reforming in Coors[31] can be extended to arbitrary hydrocarbons and to methanol, but we do not consider ammonia conversion in this fuel cell model. We allow the direct feed of fuels to the PCFC, as well as feed of reactor effluents. We assume that hydrocarbons, methanol, and carbon monoxide each undergo one net reaction, resulting in the production of carbon dioxide and hydrogen based on given conversions

$$C_nH_{2n+2}(g) + 2nH_2O_{ads} \rightarrow nCO_2(g) + (6n+2)H_{ads} \qquad \xi_{a1} = \xi_{fuel} N_{C_nH_{2n+2},feed}$$

$$CH_3OH(g) + H_2O_{ads} \rightarrow CO_2(g) + 6H_{ads} \qquad \xi_{a2} = \zeta_{fuel} N_{CH_3OH,feed}$$

$$CO(g) + H_2O_{ads} \rightarrow CO_2(g) + 2H_{ads} \qquad \xi_{a3} = \zeta_{CO} N_{CO,feed}$$

Hydrogen from the feed has to adsorb to and diffuse through the membrane. We assume that only a fraction (η_{ads}) of the inlet hydrogen will adsorb to the membrane, and a fraction (η_{diff}) thereof will diffuse to the cathode. Any hydrogen produced from reforming is produced as adsorbed hydrogen, so a fraction η_{diff} of it will diffuse. For both cases, we assume that the fraction of adsorbed hydrogen that does not diffuse fully deadsorbs from the membrane because we do not allow accumulation. Based on these assumptions, the amount of diffused hydrogen that is available on the cathode side is given by

$$N_{H,diff} = \eta_{diff} \sum_{a,r} \xi_{a,r} \nu_{H_{ads},a,r} + 2\eta_{ads}\eta_{diff} N_{H_2,feeda}$$

where the summation is over all reforming reactions at the anode a. We assume that all diffused hydrogen reacts with oxygen at the cathode side by

$$4H_{ads} + O_2(g) \rightarrow 2H_2O_{ads}$$

with an extent of reaction given by the diffusion rate of hydrogen

$$\xi_c = \frac{1}{4} N_{H,diff}$$

The modeling assumptions have the consequence that the rate of water production at the cathode is larger than the rate of water consumption at the anode. We further assume that the anode inlet stream does not contain a sufficient amount of water to reverse the presumed concentration gradient, and that all water for the reforming reactions will diffuse from the cathode to the anode, which defines

$$N_{H_2O,diff} = -\sum_{a,r} \xi_{a,r} \nu_{H_2O,a,r}$$

where the summation is again over all anode reforming reactions. Therefore, a mass balance on the cathode side yields

$$N_{H_2,outc} = N_{H_2,inc} = 0$$

$$N_{H_2O,outc} = N_{H_2O,inc} + \xi_c \nu_{H_2O} - N_{H_2O,diff}$$

$$N_{i,outc} = N_{i,inc} + \xi_c \nu_i \qquad i \neq H_2, H_2O$$

Similarly for the anode

$$N_{H_2,outa} = N_{H_2,ina} + \sum_{a,r} \xi_{a,r} \nu_{H_2,r} - N_{H_2,diff}$$

$$N_{H_2O,outa} = N_{H_2O,ina}$$

$$N_{i,outa} = N_{i,ina} + \sum_{a,r} \xi_{a,r} \nu_{i,a,r} \qquad i \neq H_2, H_2O$$

The oxygen feed to the cathode is specified relative to the stoichiometric requirement to oxidize the diffused hydrogen completely

$$N_{O_2,feedc} = \Phi \xi_c$$

We allow for a specification of water feed to the anode by requiring

$$N_{H_2O,feeda} \geq \Psi \sum_{a,r} \frac{-\nu_{H_2O,r}\xi_{a,r}}{\zeta_i} - N_{H_2O,diff}$$

where the reforming reactions are assumed to be complete. Strict inequality is observed when recycling streams or the reactor effluent stream provides sufficient water.

Solid Oxide Fuel Cell (SOFC). We simultaneously consider the possibilities of internal or external reforming, with the option of bypassing the reactor and feeding fuel directly to the fuel cell. A common presupposition[32] is to assume that carbon monoxide, hydrocarbons, and alcohols are consumed in reforming and water gas-shift reactions rather than in direct oxidation

$$CO(g) + H_2O(g) \rightarrow CO_2(g) + H_2(g) \qquad \xi_1 = \zeta_{CO} N_{CO,feed}$$

$$C_nH_{2n+2}(g) + 2nH_2O(g) \rightarrow nCO_2(g) + (3n+1)H_2(g) \qquad \xi_2 = \zeta_{fuel} N_{C_nH_{2n+2},feed}$$

$$C_nH_{2n+1}OH(g) + (2n-1)H_2O(g) \rightarrow nCO_2(g) + 3nH_2(g) \qquad \xi_3 = \zeta_{fuel} N_{C_nH_{2n+1}OH,feed}$$

To model a fuel cell that is not capable of internal reforming, one must set ζ_{fuel} and/or ζ_{CO} equal to zero. We use the notion of "equivalent hydrogen," which accounts for direct hydrogen feed as well as hydrogen produced from internal reforming of CO, hydrocarbons, or alcohols[32]

$$N_{H_2,equiv} = \zeta_{H_2} N_{H_2,feed} + \sum_{r=1}^{3} \nu_{H_2,r} \xi_r$$

The hydrogen reacts with oxygen according to

$$2H_2 + O_2 \rightarrow 2H_2O$$

with an extent of reaction defined by the equivalent hydrogen

$$\xi_4 = \frac{1}{2} N_{H_2,equiv}$$

The other extreme possibility is to assume that all components are directly oxidized in an electrochemical reaction

$$2CO(g) + O_2 \rightarrow 2CO_2(g) \qquad \xi_5 = \zeta_{CO} N_{CO,feed}$$

$$2C_nH_{2n+2}(g) + (3n+1)O_2(g) \rightarrow 2nCO_2(g) + (2n+2)H_2O(g) \qquad \xi_6 = \frac{\zeta_{fuel}}{2} N_{C_nH_{2n+2},feed}$$

$$2C_nH_{2n+1}OH(g) + 3nO_2(g) \rightarrow 2nCO_2(g) + (2n+2)H_2O(g) \qquad \xi_7 = \frac{\zeta_{fuel}}{2} N_{C_nH_{2n+1}OH,feed}$$

$$4NH_3(g) + 3O_2 \rightarrow 2N_2(g) + 6H_2O \qquad \xi_8 = \frac{\zeta_{fuel}}{4} N_{NH_3,feed}$$

We allow for either extreme; in the case of direct oxidation all electrochemical reactions are assumed to contribute to power generation

$$PW = \eta_{FC} \sum_{r=4}^{8} \xi_r \Delta_r G$$

whereas in the case of intermediate reforming reactions only the hydrogen oxidation is assumed to produce power

$$PW = \eta_{FC} \xi_4 \Delta_4 G$$

The amount of oxygen fed to the cathode is calculated relative to the stoichiometric requirement, assuming that all diffused oxygen will react in the anode

$$N_{O_2,feedc} = \Phi N_{O_2,diff} = \Phi \sum_{r=4}^{8} \xi_r$$

To prevent coking, an excess of water may be necessary. The water feed to the anode is set according to

$$N_{H_2O,feeda} \geq \Psi \sum_{r=1}^{3} \frac{-\nu_{H_2O,r} \xi_{a,r}}{\zeta_r} - \xi_4 \nu_{H_2O,4}$$

where the reforming reactions are assumed to be complete, and the produced water is assumed to be available for reforming reactions. Strict inequality is observed when recycling streams or the reactor effluent stream provides sufficient water. A mass balance on the cathode yields

$$N_{i,outc} = N_{i,inc} \qquad i = O_2$$

$$N_{O_2,outc} = N_{O_2,inc} - N_{O_2,diff}$$

and for the anode

$$N_{i,outa} = N_{i,ina} + \sum_{r=1}^{4} \xi_r \nu_{i,r} \qquad i \neq O_2$$

$$N_{O_2,outa} = N_{O_2,ina} + \sum_{r=1}^{4} \xi_r \nu_{i,r} + N_{O_2,diff}$$

Single-Chamber Fuel Cell. We consider the option of a single-chamber fuel cell that uses external reforming, resulting in an inlet feed rich in H_2 and CO. The unreacted fuel is assumed to be inert. Inlet CO is reformed by the water gas-shift reaction with extent of reaction ξ_1 according to

$$CO(g) + H_2O(g) \rightarrow CO_2(g) + H_2(g)$$

$$\xi_1 = \zeta_{CO} N_{CO,feed}$$

We again use the notion of "equivalent hydrogen," [32] here calculated as

$$N_{H_2,equiv} = \zeta_{H_2} N_{H_2,feed} + \xi_1$$

All equivalent hydrogen reacts with oxygen with an extent of reaction ξ_2 according to

$$2H_2 + O_2 \rightarrow 2H_2O$$

$$\xi_2 = \frac{1}{2} N_{H_2,equiv}$$

The water is set relative to complete reforming reaction of all components

$$N_{H_2O,feeda} \geq \Psi(N_{CO,in} + N_{CH_3OH} + 6N_{C_3H_8,in} + 8N_{C_4H_{10},in}) - \xi_2 \nu_{H_2O,2}$$

and the produced water is assumed to be available for reforming reactions.

Direct Methanol Fuel Cell (DMFC). In this type of polymer electrolyte–based fuel cell, an inlet stream of methanol and water is fed to the anode, where methanol is reformed at a relatively low temperature, around 350 K. No external reforming is required and we therefore consider only direct feed of water and methanol. Operating requirements include relatively dilute solutions of methanol in water, and major technical challenges include methanol crossover and water management.[34] At the anode we assume methanol reforming with an extent of reaction ξ_1, based on a given fuel conversion ζ_{fuel}

$$CH_3OH + H_2O \rightarrow CO_2 + 3H_2$$

$$\xi_1 = \zeta_{fuel} N_{CH_3OH,feeda}$$

A fraction $k^{trns}_{H_2}$ of the hydrogen produced by this reaction is assumed to diffuse to the cathode side

$$N^{trns}_{H_2} = k^{trns}_{H_2} \xi_1 \nu_{H_2,1} = 3k^{trns}_{H_2} \xi_1$$

The hydrogen diffusion occurs in protonic form, and electro-osmotic drag results in water transport from the anode to the cathode.[52] On the other hand, concentration gradients may result in water diffusion from the cathode to the anode, whereas electro-osmotic drag and diffusion lead to methanol transport from the anode to cathode.[52-54] For the water transport we use an effective drag coefficient that includes the electro-osmotic drag and diffusion and the overall transfer rate of water is defined relative to the proton flux

$$N^{trns}_{H_2O} = 2k^{trns}_{H_2O} N^{diff}_{H_2}$$

The coefficient $k^{trns}_{H_2O}$ can be negative or positive. We assume that a fraction $k^{trns}_{CH_3OH}$ of the unreacted methanol will diffuse from the anode to the cathode

$$N^{trns}_{CH_3OH} = k^{trns}_{CH_3OH}(1 - \zeta_{fuel}) N_{CH_3OH,feeda}$$

We assume that methanol present at the cathode will be completely[52] oxidized to CO_2 with an extent of reaction ξ_2

$$CH_3OH + 2O_2 \rightarrow CO_2 + 2H_2O$$

$$\xi_2 = N^{trns}_{CH_3OH}$$

Similarly we assume that all diffused hydrogen reacts with oxygen at the cathode with an extent of reaction ξ_3

$$2H_2 + O_2 \rightarrow 2H_2O$$

$$\xi_3 = \frac{N^{trns}_{H_2}}{\nu_{H_2,3}} = \frac{3}{2} k^{trns}_{H_2} \xi_1$$

Mass balance on the cathode side yields

$$N_{i,outc} = N_{i,inc} + \sum_{r=2,3} \xi_r \nu_{i,r} + N^{trns}_i \qquad i = H_2, H_2O, CH_3OH$$

$$N_{i,outc} = N_{i,inc} + \sum_{r=2,3} \xi_r \nu_{i,r} \qquad i \neq H_2, H_2O, CH_3OH$$

where the summation is over the two cathode reactions. Similarly for the anode

$$N_{i,outa} = N_{i,ina} + \xi_1 \nu_{i,1} - N^{trns}_i \qquad i = H_2, H_2O, CH_3OH$$

$$N_{i,outa} = N_{i,ina} + \xi_1 \nu_{i,1} \qquad i \neq H_2, H_2O, CH_3OH$$

The oxygen feed to the cathode is specified relative to the net stoichiometric requirement of the two oxidation reactions

$$N_{O_2,feedc} = -\Phi(\xi_2 \nu_{O_2,2} + \xi_3 \nu_{O_2,3})$$

The water feed to the anode is set as a multiple of the maximal water needed

$$N_{H_2O,feeda} \geq \Psi \frac{-\nu_{H_2O,1} \xi_1}{\zeta_i} + N^{trns}_{H_2O} \qquad k^{trns}_{H_2O} < 0$$

$$N_{H_2O,feeda} \geq \Psi \left(\frac{-\nu_{H_2O,1} \xi_1}{\zeta_i} + N^{trns}_{H_2O} \right) \qquad k^{trns}_{H_2O} > 0$$

where the reforming reactions are assumed complete.

Water Management. Currently direct methanol fuel cells operate with relatively dilute solutions of methanol in water, but storing a diluted methanol solution substantially reduces the energy density. Therefore, water management becomes almost mandatory; at least in theory it is possible to use the produced water to run the methanol reforming reaction. This can be done either by ensuring that diffusion of water from the anode to the cathode matches the water requirements for the methanol reforming and the electro-osmotic drag of water, or by recycling water from the cathode and/or anode effluents to the anode. The latter possibility is included as an option in the superstructure, and our model allows the first option by specifying a negative drag coefficient $k^{trns}_{H_2O}$. The overall transport of water from the cathode to the anode is limited by the production rate of water in the cathode; with simple algebraic manipulations the requirement

$$k^{trns}_{H_2O} \geq -\frac{2k^{trns}_{CH_3OH}(1 - \zeta) + 3k^{trns}_{H_2} \zeta}{6k^{trns}_{H_2} \zeta}$$

can be calculated. Water management is essentially achieved when the effective transport of water from the cathode to the anode covers the water needs for the methanol reforming reaction; in the absence of external recycling this is achieved for

$$k^{trns}_{H_2O} \leq -\frac{1}{6k^{trns}_{H_2}}$$

There are regions in the parameter space spanned by $k^{trns}_{CH_3OH}$, $k^{trns}_{H_2}$, and ζ where water management is possible only through external recycling of the anode liquids, but these are for low values of the transport coefficient $k^{trns}_{H_2} \leq 1/3$, in which case the DMFC would not operate efficiently anyway.

Changes to the hydrogen polymer electrolyte fuel cell (PEM)

For the hydrogen-based PEM fuel cell we are essentially using the model described in Mitsos et al.[10] We have added the option of net water transport

$$N^{trns}_{H_2O} = 2k^{trns}_{H_2O} N^{diff}_{H_2}$$

from the anode to the cathode. We require a water feed to the anode relative to this net transport

$$N_{\mathrm{H2O},feeda} \geq \Psi N^{trns}_{\mathrm{H_2O}}$$

Flash for separation of fuel cell effluents

We assume that the liquid and gaseous stream are in equilibrium and that the liquid stream is split into a purge stream and a recycle stream, as follows

$$N_{i,rec} = \alpha N^l_i$$

$$N_{i,purge} = N^l_i - N^l_{i,rec}$$

where α is a given split ratio. For simplicity, ideal liquid and gas phase are assumed, with supercritical components present only in the gas-phase $N^l_i = 0$, neglecting solution in the liquid phase according to Henry's law and using the Wagner equation[55] for the subcritical components. Depending on the implementation of the recycle stream, a pressure-increase mechanism (such as a pump) may be necessary. We impose an energetic penalty in terms of a compression power

$$PW = K_P \sum_i V_{m,i} N_i$$

where K_P is a parameter that needs to be specified before the simulation. K_P can be estimated by knowledge of the pressure ratio that is to be achieved and the compression efficiency.

Implementation and convergence scheme

The alternatives considered are represented as a steady-state simulation model using our in-house software packages ABACUSS II[56,57] and DAEPACK.[58,59] The mass and energy balances are formulated within the process simulator ABACUSS II, whereas the physical property calculations are performed in Fortran external procedures. The design choices are implemented within the ABACUSS model using integer variables. To facilitate the use of the model we have embedded the simulation in a web interface.[40] The requirements for the energy balance result in disjoint conditions:

IF $Q<0$ **THEN** burn no fuel **ELSE** burn enough fuel to set $Q=0$ **ENDIF**.

Similarly the water requirement ($N_{\mathrm{H_2O},in} \geq N_{\mathrm{H_2O},min}$) results in a condition $N_{\mathrm{H_2O}} = \max(0, N_{\mathrm{H_2O},min})$. Both formulations lead to nonsmooth residuals and currently the solvers have no convergence guarantees for nonsmooth functions. One way for dealing with a nonsmooth function is to use a smooth approximation,[14] but our experience shows that the water requirement does not pose significant convergence problems, whereas the energy requirement would be too difficult to formulate as a smooth function. To ensure robust convergence we remove the disjoint constraints for the energy balances and use the amount of fuels or products to be burned in each stack as a guess variable. The case of one guess variable is easy to solve because the heat load is monotonically decreasing with the flow rate and a secant method can be used. For the case of two variables we use a Broyden-like algorithm[14]; when the Broyden method calculates guess values outside the variable bounds, these guesses are replaced by the bounds. We initialize the approximate Jacobian by the negative identity matrix. This choice is motivated by the fact that the diagonal elements predominate, and the heat loads decrease with increasing guess variable ($df/dx < 0$). The convergence is sufficiently fast and robust, so that we did not implement any line search method (such as the Armijo rule).

Manuscript received July 30, 2004, and revision received Nov. 16, 2004.